which is an unusual type of fCJD [13]. The degree of the abnormalities in MRI did not correlate with the disease severity. To diagnose the slow type of CJD232, recognizing the clinical phenotype that demonstrates uncommon clinical and laboratory features found in other neurodegenerative disorders with dementia and performing genetic examination of PRNP are important.

Other characteristics of CJD232 are that CJD232 patients have no family history of CJD or dementia in either type and are reported only in Japan. More than half of genetic prion disease patients with various PRNP mutations lack family histories and the lack of family histories is not restricted to CJD232 [1]. De novo mutations [31] and very low penetration [32] are considered as the reasons. Individual PRNP mutations also show variable geographical distributions [1]. The M232R substitution may influence the disease progression because the M232R substitution extended the incubation time in an experimental transmission study using humanized knock-in mice [33]. Three suspected patients with M232R substitution but with a final diagnosis of diseases other than CJD have been reported to the Creutzfeldt-Jakob Disease Surveillance Committee, Japan because they had the M232R substitution, not because they had clinical symptoms suspecting CJD. Therefore, we think that the prevalence of 6% in 50 non-CJD patients is not the same as that of the normal Japanese population. At least, it cannot be said that all patients

having the M232R substitution demonstrate the symptoms of CJD232, and it does not seem to be supported that M232R substitution is a causative mutation. On the other hand, two probable CJD patients with M232R substitution in one family have been reported [6]. We cannot overlook these patients based on the fact that M232R substitution is very rare [4]. Whether M232R is really a causative mutation or only a rare polymorphism is another issue that needs to be resolved. We need more studies of CJD patients with M232R substitution, and especially the correlation between the pathological findings including the molecular type of PrP^{Sc} and immunohistochemical staining of PrP and the clinical findings should be clarified to determine whether it influences the disease progression. We need to study the morbidity of a population having the M232R substitution to determine whether it is a causative mutation or not.

References

1. Kovács GG, Puopolo M, Ladogana A, et al. (2005) Genetic prion disease: the EUROCJD experience. Hum Genet 118:166–174
2. Kovács GG, Trabattoni G, Heinfellner JA, Ironside JW, Knight RSG, Budka H (2002) Mutations of the prion protein gene: Phenotypic spectrum. J Neurol 249:1567–1582
3. Parchi P, Giese A, Capellari S, et al. (1999) Classification of sporadic Creutzfeldt-Jakob disease based on molecular and phenotypic analysis of 300 subjects. Ann Neurol 46:224–233
4. Kitamoto T, Ohta M, Doh-ura K, Hitoshi S, Terao Y, Tateishi J (1993) Novel missense variants of prion protein in Creutzfeldt-Jakob disease or Gerstmann-Sträussler Syndrome. Biochem Biophys Res Commun 191:709–714
5. Shimizu T, Tanaka K, Tanahashi N, Fukuuchi Y, Kitamoto T (1994) Creutzfeldt-Jakob disease with a point mutation at codon 232 of prion protein – A case report. Clin Neurol 34: 590–592

6. Hoque MZ, Kitamoto T, Furukawa H, et al. (1996) Mutation in the prion protein gene at codon 232 in Japanese patients with Creutzfeldt-Jakob disease: a clinicopathological, immunohistochemical and transmission study. Acta Neuropathol 92:441–446
7. Satoh A, Goto H, Satoh H, et al. (1997) A case of Creutzfeldt-Jakob disease with a point mutation at codon 232: Correlation of MRI and neurological findings. Neurology 49:1469–1470
8. Saito T, Isozumi K, Komatsumoto S, Nara M, Suzuki K, Doh-ura K (2000) A case of codon 232 mutation-induced Creutzfeldt-Jakob disease visualized by the MRI-FLAIR images with atypical clinical symptoms. Clin Neurol 40: 51–54
9. Tagawa A, Natsuno T, Suzuki M, Ono S, Shimizu N (2001) Creutzfeldt-Jakob disease with codon 232 point mutation and showing myoclonus and PSD in the early stage. A case report. Neurol Med 54:161–165

10. Hitoshi S, Nagura H, Yamanouchi H, Kitamoto T (1993) Double mutations at codon 180 and codon 232 of the PRNP gene in an apparently sporadic case of Creutzfeldt-Jakob disease. J Neurol Sci 120:208–212
11. Shiga Y, Miyazawa K, Sato S, et al. (2004) Diffusion-weighted MRI abnormalities as an early diagnostic marker for Creutzfeldt-Jakob disease. Neurology 63:443–449
12. Koide T, Ohtake H, Nakajima T, et al. (2002) A patient with dementia with Lewy bodies and codon 232 mutation of PRNP. Neurology 59:1619–1621
13. Jin K, Shiga Y, Shibuya S, et al. (2004) Clinical features of Creutzfeldt-Jakob disease with V180I mutation. Neurology 62:502–505
14. Goldfarb LG, Peterson RB, Tabaton M, et al. (1992) Fatal familial insomnia and familial Creutzfeldt-Jakob disease: disease phenotype determined by a DNA polymorphism. Science 258: 806–808

15. Monari L, Chen SG, Brown P, et al. (1994) Fatal familial insomnia and familial Creutzfeldt-Jakob disease: different prion proteins determined by a DNA polymorphism. Proc Natl Acad Sci 91:2839–2842

16. Barbanti P, Fabbrini G, Salvatore M, et al. (1996) Polymorphism at codon 129 or 219 of PRNP and clinical heterogeneity in a previously unreported family with Gerstmann-Sträussler-Scherinker disease (PrP-P102L mutation). Neurology 47:734–741

17. Chapman J, Arlazoroff A, Goldfarb LG, et al. (1996) Fatal insomnia in a case of familial Creutzfeldt-Jakob disease with the codon 200^{Lys} mutation. Neurology 46:758–761

18. Young K, Clark HB, Piccardo P, Dlouhy SR, Ghetti B (1997) Gerstmann-Sträussler-Scherinker disease with the PRNP P102L mutation and valine at codon 129. Molecular Brain Research 44:147–150

19. Hainfellner JA, Parchi P, Kitamoto T, Jarius C, Gambetti P, Budka H (1999) A novel phenotype in familial Creutzfeldt-Jakob disease: Prion protein gene E200K mutation coupled with valine at codon 129 and type 2 protease-resistant prion protein. Ann Neurol 45:812–816

20. Yamada M, Itoh Y, Inaba A, et al. (1999) An inherited prion disease with a PrP P105L mutation: Clinicopathologic and PrP heterogeneity. Neurology 53: 181–188

21. Teratuto AL, Piccardo P, Reich EG, et al. (2002) Insomnia associated with thalamic involvement in E200K Creutzfeldt-Jakob disease. Neurology 58:362–267

22. Doh-ura K, Tateishi J, Sasaki H, Kitamoto T, Sasaki Y (1989) Pro-leu change at position 102 of prion protein is the most common but not the sole mutation related to Gerstmann-Sträussler syndrome. Biochem Biophys Res Commun 163:974–979

23. Furukawa H, Kitamoto T, Tanaka Y, Tateishi J (1995) New variant prion protein in a Japanese family with Gerstmann-Sträussler-Scherinker syndrome. Brain Res Mol Brain Res 30:385–388

24. Shibuya S, Higuchi J, Shin RW, Tateishi J, Kitamoto T (1998) Codon 219 Lys allele of PRNP is not found in sporadic Creutzfeldt-Jakob disease. Ann Neurol 43:826–828

25. Pocchiari M, Puopolo M, Croes EA, et al. (2004) Predictors of survival in sporadic Creutzfeldt-Jakob disease and other human transmissible spongiform encephalopathies. Brain 127: 2348–2359

26. Hill AF, Joiner S, Wadsworth JD, et al. (2003) Molecular classification of sporadic Creutzfeldt-Jakob disease. Brain 126:1333–1346

27. Satoh K, Muramoto T, Tanaka T, et al. (2003) Association of an 11–12 kDa protease-resistant prion protein fragment with subtypes of dura graft-associated Creutzfeldt-Jakob disease and other prion diseases. J General Virol 84:2885–2893

28. Kitamoto T, Shin RW, Doh-ura K, et al. (1992) Abnormal isoform of prion proteins accumulates in the synaptic structures of the central nervous system in patients with Creutzfeldt-Jakob disease. Am J Pathol 140:1285–1294

29. Young GS, Geschwind MD, Fischbein NJ, et al. (2005) Diffusion-weighted and fluid-attenuated inversion recovery imaging in Creutzfeldt-Jakob disease: High sensitivity and specificity for diagnosis. Am J Neuroradiol 26: 1551–1562

30. Hamaguchi T, Kitamoto T, Sato T, et al. (2005) Clinical diagnosis of MM2-type sporadic Creutzfeldt-Jakob disease. Neurology 64:643–648

31. Dagvadorj A, Peterson RB, Lee HS, et al. (2003) Spontaneous mutations in the prion protein gene causing transmissible spongiform encephalopathy. Ann Neurol 52:355–359

32. Mitrova E, Belay Gl (2002) Creutzfeldt-Jakob disease with E200K mutation in Slovakia: characterization and development. Acta Virol 46:31–39

33. Taguchi Y, Mohri S, Ironside JW, Muramoto T, Kitamoto T (2003) Humanized knock-in mice expressing chimeric prion protein showed varied susceptibility to different human prions. Am J Pathol 163:2585–2593

Orally Administered Amyloidophilic Compound Is Effective in Prolonging the Incubation Periods of Animals Cerebrally Infected with Prion Diseases in a Prion Strain-Dependent Manner[∇]

Yuri Kawasaki,[1] Keiichi Kawagoe,[2] Chun-jen Chen,[2] Kenta Teruya,[1]
Yuji Sakasegawa,[1] and Katsumi Doh-ura[1]*

*Department of Prion Research, Tohoku University Graduate School of Medicine, Sendai, Japan,[1] and
Tokyo R & D Center, Daiichi Pharmaceutical Co., Ltd., Tokyo, Japan[2]*

The establishment of effective therapeutic interventions for prion diseases is necessary. We report on a newly developed amyloidophilic compound that displays therapeutic efficacy when administered orally. This compound inhibited abnormal prion protein formation in prion-infected neuroblastoma cells in a prion strain-dependent manner: effectively for RML prion and marginally for 22L prion and Fukuoka-1 prion. When the highest dose (0.2% [wt/wt] in feed) was given orally to cerebrally RML prion-inoculated mice from inoculation until the terminal stage of disease, it extended the incubation periods by 2.3 times compared to the control. The compound exerted therapeutic efficacy in a prion strain-dependent manner such as that observed in the cell culture study: most effective for RML prion, less effective for 22L prion or Fukuoka-1 prion, and marginally effective for 263K prion. Its effectiveness depended on an earlier start of administration. The glycoform pattern of the abnormal prion protein in the treated mice was modified and showed predominance of the diglycosylated form, which resembled that of 263K prion, suggesting that diglycosylated forms of abnormal prion protein might be least sensitive or resistant to the compound. The mechanism of the prion strain-dependent effectiveness needs to be elucidated and managed. Nevertheless, the identification of an orally available amyloidophilic chemical encourages the pursuit of chemotherapy for prion diseases.

Transmissible spongiform encephalopathies, or prion diseases, are a group of fatal neurodegenerative disorders that include Creutzfeldt-Jakob disease (CJD) and Gerstmann-Sträussler-Scheinker syndrome (GSS) in humans and scrapie, bovine spongiform encephalopathy, and chronic wasting disease in animals. These disorders are characterized by accumulation in the brain of an abnormal isoform of prion protein (PrP), which is a main component of the pathogen, prion, or a pathogen itself and which is rich in beta-sheet structure and resistant to digestion with proteinase K (24). Recent outbreaks of variant CJD and iatrogenic CJD through use of cadaveric growth hormone or dura grafts in younger people have necessitated the development of suitable therapies.

Caughey and colleagues first found Congo red and sulfated glycans to inhibit abnormal PrP formation in vitro (5, 6), although Congo red was much earlier described as a staining device for prion amyloid rods (23). Since the discovery of the therapeutic activity of Congo red, amyloidophilic compounds such as amyloid dye derivatives and glucoseaminoglycan mimetics have been noted as one class of possible therapeutic candidates for prion diseases (4, 32). Recently, the most advanced progress with amyloidophilic compounds, which have an excellent ability to permeate through the blood-brain barrier, has been made in the field of diagnosis of Alzheimer's disease. S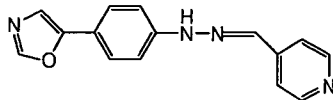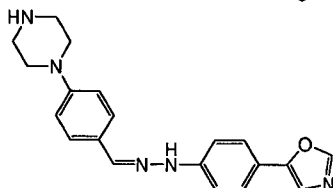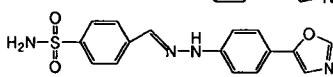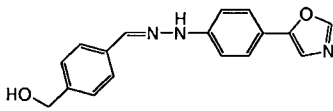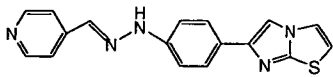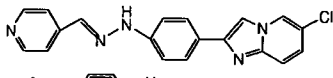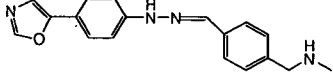ome amyloidophilic compounds are developed as imaging probes to visualize amyloid deposits in the brains of Alzheimer's disease patients using positron emission tomography or single-photon emission computed tomography technology (3). Some of these chemicals are also useful to visualize abnormal PrP amyloids of some types of prion diseases in the brain (2, 14, 15, 28, 30).

We previously reported that some of these amyloid-imaging probes are effective as antiprion compounds and prolong the incubation periods of animals cerebrally infected with prion disease (14). We also reported that a new class of amyloidophilic chemicals, styrylbenzoazole derivatives, which have better penetration through the blood-brain barrier and which show more discrete labeling of amyloid deposition in brain tissues affected by either Alzheimer's disease or prion diseases, are effective as antiprion chemicals (15, 19). However, the efficacy of these amyloidophilic compounds, intravenously administered weekly, was not remarkable but was rather limited. In addition, their effectiveness was suggested to be prion strain dependent, but this was not fully evaluated because of the limited availability of the compounds in quantity and dosing route. It can be assumed that elevated brain chemical levels are necessary for a compound's efficacy. Therefore, a multiple-dosing regimen, which causes more sustained elevation in brain chemical levels, might be preferable to a single weekly dosing. In this study, to ascertain undefined benefits and limitations of amyloidophilic compounds as therapeutic drug candidates for prion diseases, a new class of amyloidophilic compounds which have no similarity in chemical structure with previously reported antiprion compounds was synthesized and tested for either antiprion activity in vitro or therapeutic efficacy in vivo when administered orally as a mixture with feed.

* Corresponding author. Mailing address: Department of Prion Research, Tohoku University Graduate School of Medicine, 2-1 Seiryo-cho, Aoba-ku, Sendai, Miyagi 980-8575, Japan. Phone: 81-22-717-8232. Fax: 81-22-717-7656. E-mail: doh-ura@mail.tains.tohoku.ac.jp.

TABLE 1. Tested compounds and their inhibition of abnormal PrP formation in ScN2a cells

Compound	Chemical structure	Mol wt	Octanol-water distribution coefficient[a] (log $D_{6.8}$)	Inhibition of abnormal PrP (approximate EC_{50}, nM)[b]	Maximum tolerance dose[c] (μM)
cpd-B		264	4.1	0.06	>10
cpd-D1		347	2.2	100	>10
cpd-D2		342	3.6	10	>10
cpd-D3		293	3.2	1	>10
cpd-D4		319	Not determined	1	>10
cpd-D5		347	4.7	1	>10
cpd-D6		306	2.4	10	>10

[a] The distribution coefficient, a measure of a compound's hydrophilicity or hydrophobicity, was estimated using ChemAxon's calculator plugin software (Budapest, Hungary). The coefficients of medicines used for brain diseases are generally around 3.0.
[b] The approximate dose giving 50% inhibition of abnormal PrP formation relative to the control.
[c] The maximal dose that does not affect the rate of cell growth to confluence.

MATERIALS AND METHODS

Chemicals and experimental models. Test compounds were synthesized at the Tokyo R & D Center of Daiichi Pharmaceutical Co., Ltd. (Tokyo, Japan). The structures of the compounds are shown in Table 1. The compounds were dissolved in 100% dimethyl sulfoxide using ultrasonication and stored at −30°C until use.

Cultured cells were grown in Opti-MEM (Invitrogen Corp., Carlsbad, CA) supplemented with 10% fetal calf serum. As cellular models for the screening of antiprion compounds, either mouse neuroblastoma cells (N2a cells) or N2a cells with fivefold PrP overexpression (N2a-58 cells) which were persistently infected with a distinct prion strain were used, as follows: N2a cells infected with RML scrapie prion (ScN2a cells) (25), N2a cells with 22L scrapie prion (N167 cells), N2a-58 cells with RML scrapie prion (N002 or Ch2 cells), or N2a-58 cells with Fukuoka-1 GSS prion (F3 cells) (15). The Ch2 cells are a subclone of N002 cells.

Five-week-old Tga20 mice overexpressing murine PrP (11) or Tg7 mice overexpressing hamster PrP (26) were used as animal disease models after intracerebral infection with 20 μl of 1% (wt/vol) brain homogenate of RML prion, 22L prion, or Fukuoka-1 prion for Tga20 mice or 263K scrapie prion for Tg7 mice. Five-week-old ICR mice and Syrian hamsters were also used after they were infected intracerebrally with 20 μl of 1% (wt/vol) brain homogenate of RML prion or 40 μl of 1% (wt/vol) brain homogenate of 263K prion, respectively. Each animal was maintained under deep ether anesthesia for minimum distress during intracerebral inoculation. Permission for the animal study was obtained from the Animal Experiment Committee of Tohoku University, Japan.

In vitro PrP imaging. Autopsy-diagnosed brain samples from cases of GSS, which were kindly provided by Toru Iwaki from the Department of Neuropathology, Kyushu University, Japan, were used. After fixation in 10% buffered formalin for 2 weeks, the sample was immersed in 98% formic acid for reduction of prion infectivity, embedded in paraffin, and cut into 7-mm-thick sections. For neuropathological staining, deparaffinized sections were immersed in 1% Sudan

black solution to quench tissue autofluorescence. They were then incubated for 30 min in 1 mM solution of compound B (cpd-B), rinsed with distilled water, and examined under a fluorescence microscope (DMRXA; Leica Microsystems GmbH, Wetzlar, Germany) using a fluorescein isothiocyanate filter set.

For comparison, each section was subsequently immunostained for PrP as described in a previous study (7). Briefly, the sections were treated with a hydrolytic autoclave and incubated with a rabbit primary antibody, anti-PrP-C, which was raised against a mouse PrP fragment consisting of amino acids 214 to 228 (1:200; Immuno-Biological Laboratories Co. Ltd., Gunma, Japan), followed by incubation with EnVision+System horseradish peroxidase labeling polymer (Dako, Glostrup, Denmark). The reaction product was developed with 3,3'-diaminobenzidine tetrahydrochloride solution and counterstained with hematoxylin.

In vitro treatment in cell cultures. Antiprion activity was evaluated by assaying the content of protease-resistant PrP (PrPres) in the cellular models, as described in earlier studies (6, 8, 18). Briefly, test compounds were added at the designated concentrations when cells were passaged at 10% confluence, while maintaining the final concentration of dimethyl sulfoxide in the medium at less than 0.5%. The cells were allowed to grow to confluence and were lysed with lysis buffer (0.5% sodium deoxycholate, 0.5% Nonidet P-40, phosphate-buffered saline [PBS]). For analysis of PrPres, samples were digested using 10 μg/ml proteinase K for 30 min at 37°C; the digestion was stopped using 1 mM phenylmethylsulfonyl fluoride. The samples were centrifuged at 100,000 × g for 30 min, and then pellets were resuspended in 1× sample loading buffer and boiled for 5 min. For analysis of the total level of cellular PrP in N2a cells treated with a test compound, cell lysates were mixed directly with one-quarter volume of 5× sample loading buffer and boiled for 5 min.

The samples were analyzed by immunoblotting. They were separated by electrophoresis on a 15% Tris-glycine–sodium dodecyl sulfate-polyacrylamide gel and electroblotted onto a polyvinylidene difluoride filter. The PrP was detected

using a monoclonal antibody, SAF83 (1:5000; SPI-Bio, Massy, France), followed by an alkaline phosphatase-conjugated goat anti-mouse antibody (1:20,000; Promega Corp., Madison, WI). Immunoreactivity was visualized using a CDP-Star detection reagent (Amersham, Piscataway, NJ). More than three independent assays were performed in each experiment.

The cell surface level of cellular PrP was assayed using flow cytometry, as described previously (10). Briefly, N2a cells dispersed by treatment with 0.1% collagenase (Wako Pure Chemical Industries Ltd., Osaka, Japan) were washed with ice-cold 0.5% fetal calf serum in PBS and incubated with SAF83 (1:500) or isotype-matched control immunoglobulin G1 for 20 min on ice. Cells were washed with 0.5% fetal calf serum in PBS and incubated with goat F(ab')2 fragment anti-mouse immunoglobulin G (heavy plus light chain)-phycoerythrin (1:100) (Beckman Coulter Inc., CA) for 20 min on ice. After washing, cells were analyzed using an EPICS XL-ADC flow cytometer (Beckman Coulter Inc., CA).

Pharmacokinetic studies. Brain cpd-B levels in the animals were assayed as described previously (20) after a 1-week feeding with 0.2% cpd-B ad libitum. All animals were sacrificed at 9:00 a.m. of day 8 by excision of the carotid artery under deep ether anesthesia to remove as much blood as possible, and the brain was collected, rinsed with saline, and weighed. Because preliminary studies found no significant difference in the data for perfused brains and nonperfused brains, the brain was not perfused with saline to remove residual blood. The brain was homogenized with 2 ml of 100% methanol for mouse brain or 4 ml for hamster brain. After centrifugation of the homogenate at 800 $\times$ g for 10 min, the supernatant was diluted with 9 volumes of 20 mM phosphate buffer, pH 6.5 (PB), and then filtered to obtain the sample for analysis. The sample was then applied to a conditioned C_{18} solid-phase extraction cartridge. The compound was eluted with methanol and was diluted with an equal volume of PB. The compound then was separated by high-performance liquid chromatography using a reversed-phase column (C_4, 4.6 $\times$ 150 mm; Phenomenex Inc., Torrance, CA). The compound was detected using a UV detector at 285 nm, and the dose of cpd-B per gram of brain tissue was determined.

The kinetics of brain uptake and washout of cpd-B were also investigated as described previously (20). The compound was solubilized in 5% Tween 80 in ethanol and then prepared as a 0.2-mg/ml solution containing 5% Tween 80 and 5% ethanol in saline. The compound at a dose of 1.0 mg/kg of body weight was administered intravenously to ICR mice under ether anesthesia. Both Tween 80 and ethanol are FDA-approved solubilizers of lipophilic medicinal chemicals. At the dose used in the study, neither solubilizer has been reported to cause any toxicity or to affect the pharmacokinetics. At 2 min or 30 min after injection, the blood was collected from the heart using heparin, and then the brain was obtained as described above. The blood plasma was mixed with 3 volumes of acetonitrile and centrifuged at 10,000 $\times$ g for 5 min. The supernatant was mixed with the same volume of PB and subsequently filtered to obtain the plasma sample for analysis. The preparation for the brain sample for analysis and the assay of the samples were performed as described above. The percentage of the injected dose per gram of tissue or fluid was used as a measure of the brain or plasma level of the compound.

In vivo treatment in animal models. In experimental animals that had been infected intracerebrally with a prion pathogen, cpd-B was given orally ad libitum as a mixture with powder feed at doses of 0.1%, 0.13%, 0.2%, and 0.33% by weight in the feed, corresponding, respectively, to ca. 150 mg/kg of body weight/day, ca. 225 mg/kg of body weight/day, ca. 300 mg/kg of body weight/day, and ca. 500 mg/kg of body weight/day in Tga20 mice, as each mouse consumed an average of 3.75 g of the feed per day. The animals were monitored every day until the terminal stage of disease; the incubation period, which was defined in the present study as the length of time from inoculation to the terminal stage of disease, was determined.

Pathological and infectivity assays. The right brain hemispheres of the mice were fixed using 10% buffered formalin and then embedded in paraffin. Three-micrometer-thick sections of the coronal slice sited at around one-third of the distance from the interaural line to the bregma line were dewaxed and immunostained using an anti-PrP-C antibody, as described above, or an antibody against glial fibrillary acidic protein (1:5,000; Dako, Glostrup, Denmark), as described in a previous study (9).

For detection of PrPres by immunoblotting, the left brain hemisphere was homogenized with 9 volumes of lysis buffer; after low-speed centrifugation, the supernatant was treated with 50 μg/ml proteinase K for 30 min at 37°C. An aliquot corresponding to 0.13 mg of brain tissue for PrPres assay or 0.83 μg of brain tissue for total PrP assay was electrophoresed on a 13.5% Tris-glycine–sodium dodecyl sulfate-polyacrylamide gel and analyzed by immunoblotting as described above.

For the infectivity assay, the left brain hemisphere was homogenized with PBS to produce a 10% brain homogenate. Serially diluted homogenate samples for

assay were produced by diluting the brain homogenate serially with 10% brain homogenate of noninfected mice fed with 0.2% cpd-B for 1 month. A 20-μl aliquot of each sample was then inoculated intracerebrally into each of the Tga20 mice. Incubation times were assayed as described above.

Statistical analysis. Statistical significance was analyzed using the Kruskal-Wallis test followed by Scheffè's F test for multiple comparisons. Correlation analysis was performed using Spearman's rank correlation coefficient method. The regression coefficient was determined using simple linear regression analysis. The survival rate was calculated using the Kaplan-Meier method; its significance was evaluated using the log rank method.

RESULTS

Antiprion activity in vitro. The antiprion activities of newly synthesized compounds were investigated using ScN2a cells, which are N2a cells that are persistently infected with RML scrapie prion and are commonly used for drug screening. At a half-maximum effective concentration (EC_{50}) of about 60 pM, cpd-B inhibited PrPres formation (Table 1 and Fig. 1A). Other related compounds were also potent within a nontoxic dose range of up to 10 μM.

To investigate whether the efficacies of the compounds depend on the pathogen strain, cpd-B was tested in four other cell lines that had been infected individually with distinct prion strains. As shown in Fig. 1A, cpd-B was effective only in N002 (EC_{50}, 320 nM) and Ch2 (EC_{50}, 300 nM), both of which are N2a-58 cells infected with RML prion. However, the inhibitory activity in these cells was not as strong as that in ScN2a cells, which are derived from N2a cells expressing one-fifth of the normal PrP molecules of N2a-58 cells. In contrast, cpd-B was ineffective in both N167 cells (N2a cells infected with 22L scrapie prion) and F3 cells (N2a-58 cells infected with Fukuoka-1 GSS prion) at a dose of less than 10 μM. However, at a dose of 10 μM, a marginal reduction of the PrPres signals was observed in both cells. At a dose of greater than 10 μM, cell toxicity was observed. The results suggest that cpd-B exerts an inhibitory activity on PrPres formation in a prion strain-dependent manner: more effectively for RML prion and marginally for 22L prion or Fukuoka-1 prion.

The inhibition mechanism included no alteration of either the total or the cell surface level of normal PrP, as demonstrated in noninfected N2a cells treated with 1 μM cpd-B, using either immunoblot analysis of the cell lysate without protease digestion or flow cytometry analysis of the cell surface PrP (Fig. 1B and C). In addition, cpd-B did not facilitate the digestion of abnormal PrP by proteinase K, nor did it interfere with immunodetection, because PrPres signals were not modified after cpd-B was mixed and incubated with a cell lysate of nontreated ScN2a cells before proteinase K digestion (data not shown).

Pharmacological properties. Abnormal PrP amyloid imaging by cpd-B was performed on brain sections of GSS cases to examine the amyloidophilic properties of cpd-B. The compound bound to and fluorescently labeled most of the PrP plaques in cerebellar cortices of GSS cases (Fig. 1D). Background staining was barely observed after rinsing off the excess compound. Immunohistochemical analysis of PrP revealed that the compound achieved high-specificity labeling. The compound displayed no signal in control sections without amyloid lesions (data not shown).

Next, to examine the brain accessibility of cpd-B when administered orally, brain levels of cpd-B in the experimental
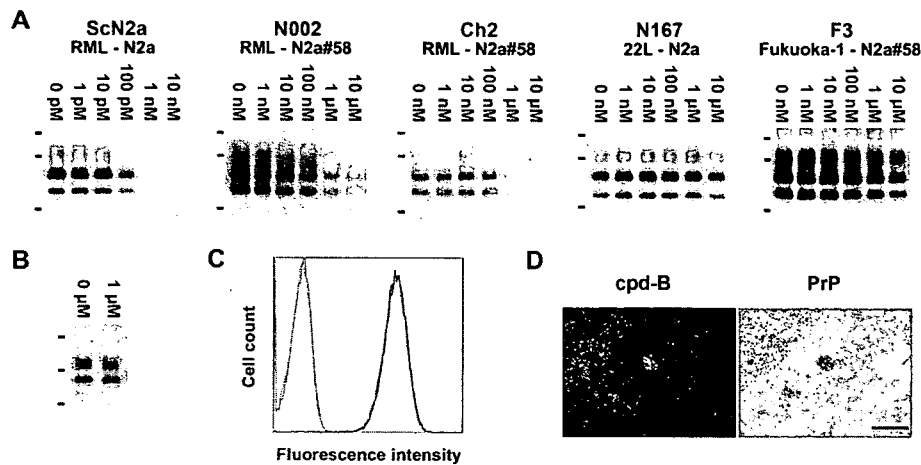
FIG. 1. cpd-B effects on prion-infected and noninfected cells and its amyloidophilic property. (A) Immunoblot analyses of PrPres formation in various prion-infected cells treated with the indicated concentrations of cpd-B. N2a-58 (N2a#58) is a stable transformant of N2a and expresses five-times-higher levels of PrP than N2a. Ch2 is a subclone of N002. The bars on the left are molecular size markers for 41, 32, and 18 kDa. (B) Immunoblot analysis of total normal PrP in noninfected N2a cells treated with cpd-B. Molecular size markers on the left are 47, 32, and 25 kDa. (C) Flow cytometric analysis of cell surface-normal PrP in noninfected N2a cells treated with 1 μM cpd-B. The solid and broken lines, respectively, indicate cpd-B-treated cells and nontreated cells. Gray line peaks on the left show their respective controls, using isotype immunoglobulin as a first antibody. (D) Imaging of abnormal PrP plaques in the brain tissue by cpd-B. Abnormal PrP deposition in a cerebellar tissue from a case of GSS was fluorescently labeled with cpd-B and subsequently immunostained with an anti-PrP antibody. Bar, 50 μm.

animals used in the study were assayed after the animals were fed ad libitum with 0.2% cpd-B-containing feed for 1 week. The brain level of cpd-B was 39.16 ± 22.15 nmol/g brain tissue in Tga20 mice ($n = 4$), 26.04 ± 12.50 nmol/g brain tissue in ICR mice ($n = 4$), and 22.94 ± 7.64 nmol/g brain tissue in Tg7 mice ($n = 4$). Syrian hamsters, however, showed a lower level, 7.26 ± 2.47 nmol/g brain tissue ($n = 4$). A considerable amount of cpd-B was detected in the brains of all experimental animals; no significant difference in the brain cpd-B levels was found among the types of the mice.

Further study of the pharmacokinetics of cpd-B in the blood and the brain was performed with ICR mice after cpd-B was injected into the tail vein. The percentage of the injected dose per gram of tissue or fluid was determined. The brain uptake level of cpd-B at 2 min after intravenous injection was $8.01\% \pm 1.27\%$ of the injected dose/g tissue, whereas the blood plasma level was $2.92\% \pm 1.00\%$/g fluid. Consequently, the ratio of the cpd-B concentration in the brain to that in the blood plasma is 2.7:1, indicating that cpd-B is equal to the best brain-entering amyloidophilic chemicals previously identified (15). On the other hand, both the brain level and the blood plasma level of cpd-B at 30 min after the intravenous injection were below the measurable level of 50 pM, which indicates that cpd-B is very rapidly washed out from the brain and blood.

Regarding toxicity of cpd-B, body weight losses of about 16% in Tga20 mice and about 5% in Tg7 mice were observed after cpd-B was given orally ad libitum for 1 week at a dose of 0.33% weight in feed, which corresponds to ca. 500 mg/kg of body weight/day. Other doses of cpd-B tested in this study produced no apparent toxic effects in the experimental animals used.

Therapeutic efficacy in vivo. The therapeutic activity of cpd-B in vivo was assayed in murine PrP-overexpressing Tga20 mice that had been cerebrally infected with RML scrapie prion. The nontreated infected mice started exhibiting abnor-

mal clinical signs such as staggering, rotating, irritation, and motionlessness at about 2 months after the infection; the mice then wasted into the terminal stage of disease in a week. Treatment by feeding cpd-B-containing feed ad libitum was initiated immediately after the infection and continued until the terminal stage of disease. The cpd-B-treated mice did not exhibit such abnormal signs as described above and wasted gradually into the terminal stage of disease. As shown in Fig. 2A, oral cpd-B treatment significantly prolonged the incubation periods of infected Tga20 mice in a dose-dependent manner; these were 68.5 ± 5.9 days in the nontreated control mice, 108.0 ± 2.8 days in the mice treated with 0.1% cpd-B feed, 120.5 ± 10.7 days in the mice with 0.13% cpd-B feed, and 154.3 ± 19.9 days in the mice with 0.2% cpd-B feed. Therefore, oral cpd-B treatment at the highest dose produced a 2.3-fold extension of the incubation periods of the mice. Statistical analyses demonstrated a significant linear correlation between the incubation periods and the cpd-B doses ($r = 0.95$; $P < 0.01$); the correlation equation was $y = 426.37x + 66.93$ (y, incubation period [days]; x, cpd-B dose [percentage in feed]), and the correlation coefficient was 0.89 ($P < 0.01$).

In our previous studies, the effectiveness of amyloidophilic chemicals in the extension of incubation periods of infected animals was observed only in Tga20 mice infected with RML prion (14, 15). ICR mice were then examined for the therapeutic efficacy of oral cpd-B treatment to investigate whether effectiveness of amyloidophilic compounds is restricted only to Tga20 mice. Nontreated control ICR mice that had been cerebrally infected with RML prion were in the terminal stage of disease at 154.2 ± 18.4 days postinfection, whereas the mice treated with 0.2% cpd-B feed lived significantly longer ($P < 0.01$). Even though the oral cpd-B treatment was discontinued at day 187 postinfection when the last of the nontreated animals reached the terminal stage of disease, more than half of the treated mice survived to day 270 postinfection (Fig. 2B).

A Tga20-RML model

B ICR-RML model

C Tga20-22L model

D Tga20-Fukuoka-1 model

E Tg7-263K model
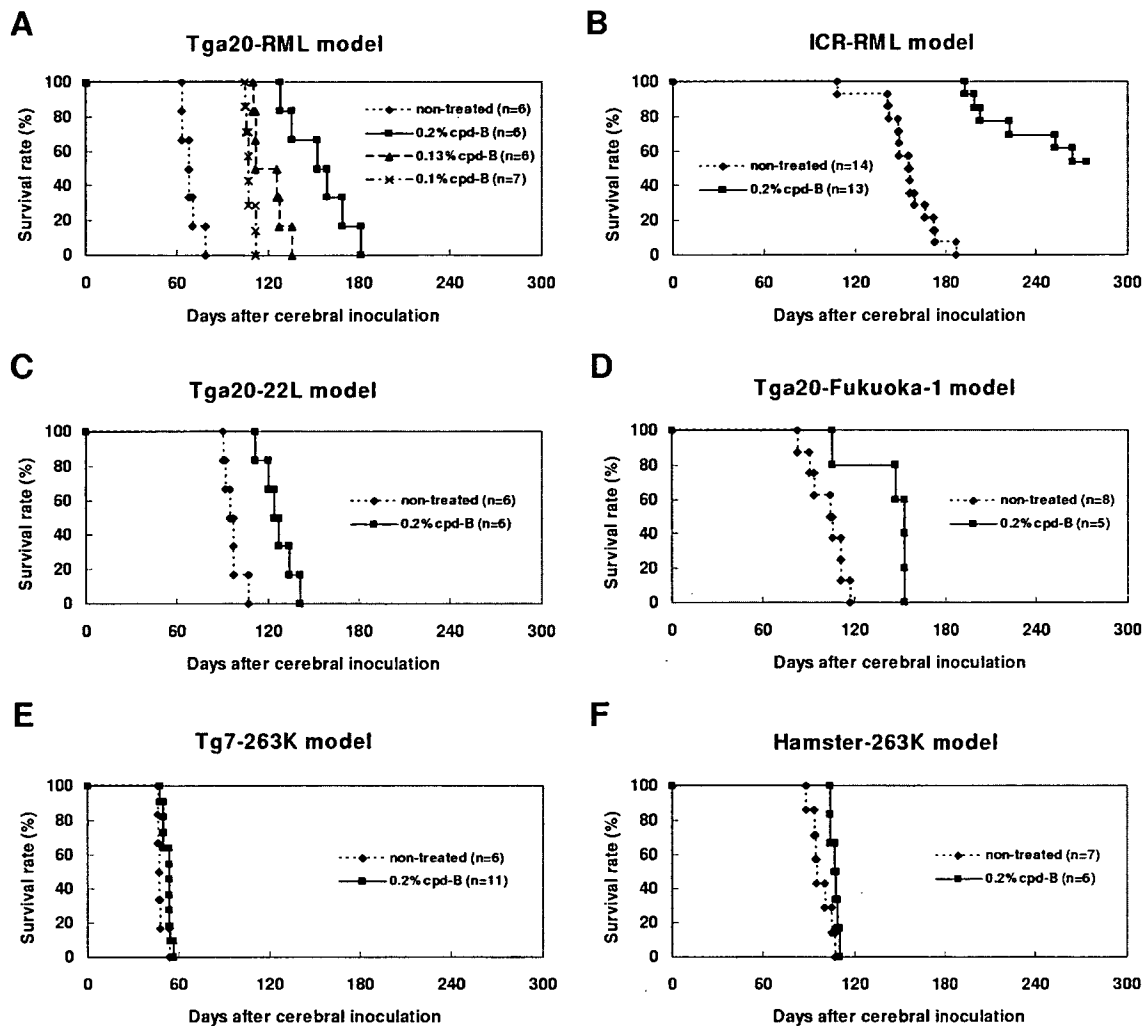
F Hamster-263K model

FIG. 2. Effects of orally administered cpd-B on animals cerebrally infected with prion diseases. cpd-B was given orally in a mixed form with powder feed ad libitum throughout the incubation periods in all animal disease models except the ICR-RML model, in which oral cdp-B treatment was discontinued at the time when the last of the nontreated animals reached the terminal stage of disease. In this study, the incubation periods are defined as the periods from the cerebral infection to the terminal stage of disease. Survival rates were calculated using the incubation periods and are plotted using the Kaplan-Meier method.

Next, the therapeutic efficacy of oral cpd-B treatment against other prion strains was investigated. The cpd-B treatment significantly prolonged the incubation periods of Tga20 mice that had been cerebrally infected with 22L scrapie prion ($P < 0.01$); these were 96.3 ± 5.9 days in the nontreated control mice and 126.3 ± 10.3 days in the mice treated with 0.2% cpd-B feed, indicating a 1.3-fold extension of the incubation period (Fig. 2C). Control mice started exhibiting distinguished opisthotonus with head rotating a week before the terminal stage of disease, whereas cpd-B treated mice showed no such clinical sign, even in the terminal stage.

cpd-B was also effective against Fukuoka-1 GSS prion. Cerebrally infected Tga20 mice lived significantly longer with oral cpd-B treatment ($P < 0.05$), i.e., 101.6 ± 12.1 days for the nontreated control mice and 142.2 ± 21.0 days for the mice treated with 0.2% cpd-B feed, indicating a 1.4-fold extension of the incubation period (Fig. 2D). Staggering was observed as an initial clinical sign in the control mice more than 1 week before

the terminal stage of disease, although this clinical sign was not seen in the cpd-B treated mice.

In contrast to the case for these prion strains, the efficacy of oral cpd-B treatment was very marginal for 263K scrapie prion when Tg7 mice expressing hamster PrP were used as the host (Fig. 2E). The incubation periods of the cpd-B-treated mice (52.7 ± 2.8 days) were significantly but very marginally longer than those of the nontreated mice (48.0 ± 3.0 days) ($P < 0.05$). This prion is a hamster-adapted scrapie prion strain; Syrian hamsters were used as the host to examine whether the marginal efficacy of oral cpd-B treatment is attributable chiefly to the host Tg7 mouse or to the pathogen strain 263K prion. As observed in Tg7 mice, hamsters treated with 0.2% cpd-B feed also exhibited a marginal increase in the incubation period compared to that of the nontreated control hamsters that had been cerebrally infected with 263K prion ($P < 0.05$): 107.0 ± 2.5 days in the cpd-B treated hamsters and 97.4 ± 6.9 days in the non-
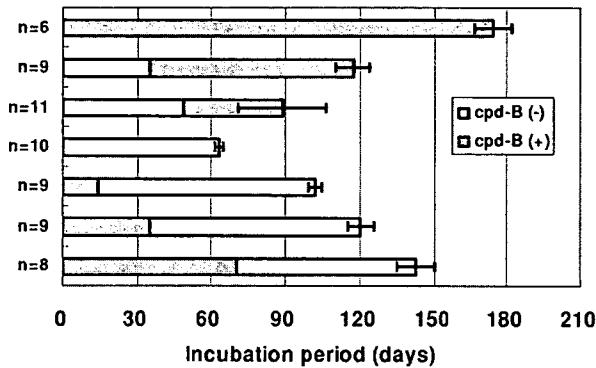
FIG. 3. cpd-B effects throughout various timings and durations of oral administration. Tga20 mice cerebrally infected with RML prion were treated with 0.2% cpd-B feed at different times and for different durations, and the incubation periods were assayed. Open bars indicate the durations of no treatment [cpd-B (−)]. Shaded bars indicate the durations of oral cpd-B treatment [cpd-B (+)].

treated hamsters (Fig. 2F). These results indicate that oral cpd-B treatment is not as effective for 263K prion.

Timing and duration of dosing. The effectiveness of cpd-B at various timings and durations of oral administration was analyzed in Tga20 mice that had been cerebrally infected with RML prion (Fig. 3). The incubation periods of the nontreated mice were 63.0 ± 1.8 days, whereas the incubation periods of the mice treated with 0.2% cpd-B feed were inversely correlated with the postinfection durations to the commencement of cpd-B treatment ($r = -0.79$; $P < 0.01$): 174.5 ± 7.6 days when started at day 0 postinfection, 117.2 ± 7.0 days when started at day 35 postinfection, and 88.7 ± 17.3 days when started at day 49 postinfection. On the other hand, the incubation periods of the mice treated with 0.2% cpd-B feed were also correlated with the durations of cpd-B treatment which started immediately after cerebral infection ($r = 0.95$, $P < 0.01$): 102.1 ± 2.9 days when treated for 14 days from the infection, 120.2 ± 5.2 days when treated for 35 days from the infection, and 142.5 ± 7.8 days when treated for 70 days from the infection. In addition, when the cpd-B treatment was discontinued during early disease stages, the remaining incubation times were longer than that of the control mice.

Pathological evaluation. The PrPres content in the brains of cpd-B-treated mice was analyzed sequentially by immunoblotting and compared with that in the nontreated control mice (Fig. 4A). The PrPres signals in the nontreated mice were very strong at the terminal stage of disease (day 63 postinfection). In contrast, in the mice treated with 0.1% cpd-B feed from the start of infection, PrPres signals were faint at day 63 postinfection and distinct at the terminal stage of disease (day 108 postinfection). However, the PrPres signals at the terminal stage of disease did not reach the high level shown by the nontreated control mice at that stage. Comparison of the signal intensities of the diglycosylated PrPres form showed that 6- to 15-fold-diluted samples from the nontreated terminal mice exhibited signal intensities similar to those of undiluted or 2-fold-diluted samples from the 0.1% cpd-B-treated terminal mice (Fig. 4B). Similarly, in the mice treated with 0.2% cpd-B feed from the start of infection, PrPres signals gradually increased according to the time course after infection: no signals

were detected at day 63 postinfection, distinct signals were detected at day 120, and similar or more distinct signals were detected at the terminal stage of infection (day 154 postinfection). The PrPres signal levels of the 0.2% cpd-B-treated mice at the terminal stage of disease were indistinguishable from those of the 0.1% cpd-treated mice at the terminal stage of disease.

The glycoform patterns of PrPres differed completely. As shown in Fig. 4B, when the samples were diluted and reassayed so that the signal intensities of diglycosylated PrPres forms were equalized as much as possible, the difference was much more distinct. The glycoform patterns in the nontreated mice, which were uniform in the analyzed samples, were predominantly monoglycosylated, whereas the glycoform patterns in the cpd-B-treated mice were not necessarily uniform but were always predominantly diglycosylated. This predominance of diglycosylated PrPres was also observed for 263K prion (Fig. 4C) but not for other prion strains used in this study (data not shown).

Modification in the pathology of the brains of cpd-B-treated mice was analyzed (Fig. 4D). For nontreated control mice with an incubation period of 63 days, the brain showed prominent pathological changes consisting of abnormal PrP deposition and glial cell reaction in the thalamus, although the brains of the mice treated with 0.2% cpd-B feed showed no such pathological changes at day 63 postinfection and milder levels of abnormal PrP deposition at the terminal stage of disease (day 154 postinfection). No difference was apparent in the pattern or distribution of abnormal PrP deposition in the brains between the nontreated mice and the cpd-B-treated mice.

Infectivity analysis. Infectivity levels are inversely correlated with incubation periods (24). Therefore, infectivity levels of the brains of the mice treated with 0.2% cpd-B feed were evaluated by assaying the incubation periods of animals that had been cerebrally inoculated with the brain homogenate (Table 2). The 10^2-fold-diluted brain homogenates from the cpd-B-treated mice at day 63 postinfection exhibited incubation periods similar to those of the 10^5-fold- or greater diluted brain homogenates from the nontreated mice; the 10^2-fold-diluted brain homogenates from the cpd-B-treated mice at the terminal stage of disease (day 154 postinfection) showed incubation periods similar to those of the 10^4-fold- or 10^5-fold-diluted brain homogenates from the nontreated mice. The data indicate that the brains of mice treated with 0.2% cpd-B feed had much lower infectivity levels than those of the nontreated mice at the same time point after infection and even at the terminal stage of disease. A 100-fold to 1,000-fold difference in infectivity levels was apparent between the nontreated terminal mice and the cpd-B-treated terminal mice, although a less-than-100-fold difference in PrPres levels between the two mouse groups was estimated from the immunoblot data shown in Fig. 4B. On the other hand, no inconsistency was apparent in the gaps in the infectivity levels and the PrPres levels between the cpd-B-treated mice at day 63 postinfection and those at the terminal stage of disease. The gap in infectivity levels between these two groups was around 10-fold; 10-fold dilution of the samples from the cpd-B-treated terminal mice similarly produced no signals on the immunoblot, as observed in the samples from the cpd-B-treated mice at day 63 postinfection (data not shown).
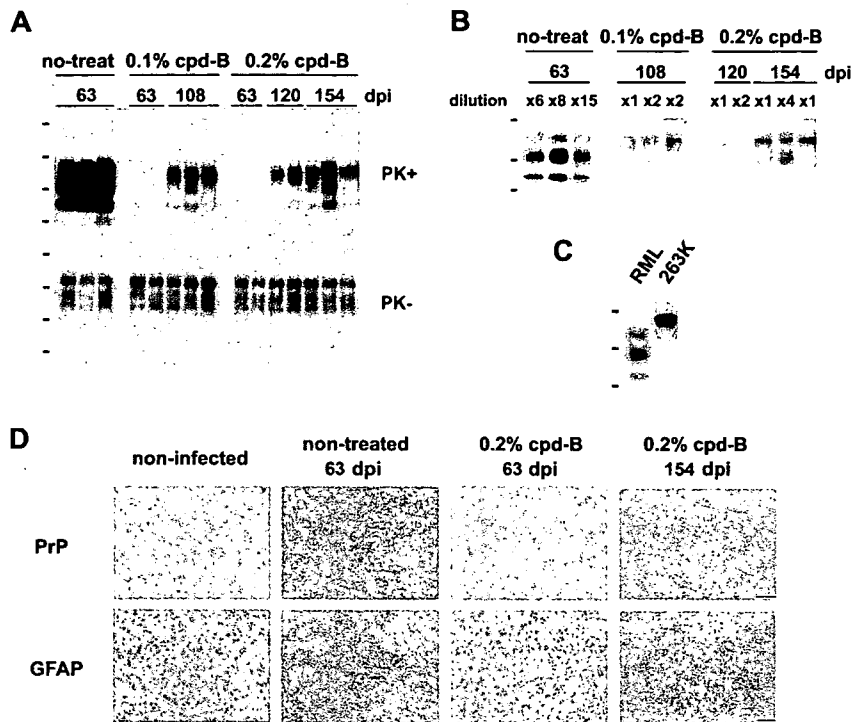
FIG. 4. Immunoblot and immunohistochemical analyses of cpd-B-treated animal brains. (A) Immunoblot analysis of PrP in the brains of nontreated mice (no-treat) or mice treated with 0.1% cpd-B feed or 0.2% cpd-B feed. Each lane represents an aliquot corresponding to 0.13 mg for PrPres (PK+) or 0.83 μg for total PrP (PK−) of brain tissue from each mouse sacrificed at a designated day after cerebral infection (dpi). Molecular size markers on the left show 47, 32, 25, and 16 kDa. (B) Immunoblot analysis of PrPres of some of the samples in panel A, which were diluted and reassayed to equalize signal intensities of the diglycosylated PrPres bands as much as possible for comparison of the signal intensity and the glycoform pattern of PrPres. Molecular size markers on the left show 32, 25, and 16 kDa. (C) Immunoblot analysis of PrPres to compare the glycoform patterns of the RML prion and the 263K prion. Analyzed samples were from an RML prion-infected mouse brain and a 263K prion-infected hamster brain. Molecular size markers on the left are the same as those in panel B. (D) Immunohistochemical analysis of abnormal PrP deposition (PrP) and neurodegenerative changes by means of astrocytic glial reaction (glial fibrillary acidic protein [GFAP]) in the brains of noninfected mice, infected but nontreated mice, and infected mice treated with 0.2% cpd-B feed. Data from each representative mouse sacrificed at a designated day after cerebral infection (dpi) are shown; every picture was taken from an almost identical area of the thalamus. The samples of 0.2% cpd-B at 63 dpi and 0.2% cpd-B at 154 dpi are from the same individual mouse as the samples in the right lane of 0.2% cpd-B 63 dpi and the rightmost lane of 0.2% cpd-B 154 dpi in panel A, respectively. Bar, 50 μm.

DISCUSSION

In this study, the newly synthesized chemical cpd-B was discovered as an orally available antiprion compound that is effective for prolonging the incubation periods of animals cerebrally infected with prion diseases. This compound has no similarity in chemical structure to previously reported antiprion compounds, although the compound shares the following properties with antiprion amyloidophilic chemicals we previously reported, such as (trans, trans)-1-bromo-2,5-bis-(3-hydroxycarbonyl-4-hydroxy)styrylbenzene and styrylbenzoazole chemicals: binding to PrP amyloid plaques in the brain tissue, inhibiting abnormal PrP formation in prion-infected cells without any effect on either normal PrP expression level or protease sensitivity of abnormal PrPres, preferential antiprion effects in RML prion-infected cells rather than 22L prion-infected or Fukuoka-1 prion-infected cells, and prolonging the incubation period in the RML prion-infected Tga20 mouse model but never or only marginally in the 263K prion-infected Tg7 mouse model. The discovery of orally available cpd-B effectiveness reinforces the idea that amyloidophilic chemicals can serve as one class of antiprion drug candidates.

This study has shown that prion strains are definitely influential in the outcome of the treatment with antiprion compounds. Treatment with cpd-B was effective against all tested prion strains, but both its antiprion effectiveness in vitro and its therapeutic efficacy in vivo were consistently dependent on the prion strain. In fact, cpd-B was most effective against RML prion but less effective against 22L prion and Fukuoka-1 prion either in vitro or in vivo. In addition, its lowest effectiveness in therapeutic efficacy was demonstrated identically in either the 263K prion-infected Tg7 mouse model or the 263K prion-infected hamster model, although its effectiveness against 263K prion could not be evaluated on the same host background as that used for the other prion strains. It is unlikely that differences in the hosts used in this study are influential in the therapeutic efficacy of cpd-B treatment, because the brain chemical levels in all types of mice fed with 0.2% cpd-B for 1 week were not significantly different.

Amyloidophilic chemicals are not the only class of antiprion compound that exhibits the therapeutic efficacy in a prion strain-dependent manner. The polyene antibiotic amphotericin B is another example, but it is opposite to amyloidophilic chemicals and is specifically effective against 263K prion (1).

TABLE 2. Infectivity assays of the brains of nontreated mice or cpd-B-treated mice

Dilution	Nontreated mice (63 dpi[a])			cpd-B treated mice (63 dpi)			cpd-B treated mice (154 dpi)		
	Mouse no.	No. of diseased mice/total	Mean incubation time (days) ± SD	Mouse no.	No. of diseased mice/total	Mean incubation time (days) ± SD	Mouse no.	No. of diseased mice/total	Mean incubation time (days) ± SD
10^2	cnt-1	8/8	77.4 ± 4.5	bc-1[d]	7/7	284.1 ± 54.6	bl-1	7/7	122.0 ± 14.0
				bc-2[e]	8/8	136.8 ± 19.2	bl-2[f]	7/7	92.6 ± 8.9
							bl-3	7/7	89.1 ± 4.0
10^3	cnt-1	8/8	84.4 ± 6.9	bc-1[d]	0/7	>140[c]	bl-1	5/9	>140[c]
	cnt-2	6/6	75.3 ± 2.4	bc-2[e]	1/8	>140[c]	bl-2[f]	7/7	97.4 ± 9.6
	cnt-3	7/7	75.7 ± 7.4				bl-3	9/9	101.6 ± 7.4
10^4	cnt-1	7/7	88.4 ± 7.3	bc-1[d]	1/8	>140[c]	bl-1	1/9	>140[c]
				bc-2[e]	1/9	>140[c]	bl-2[f]	3/7	>140[c]
							bl-3	3/7	>140[c]
10^5	cnt-1	6/6	155.7 ± 55.3						
	cnt-2	7/7	105.4 ± 16.5						
	cnt-3	7/7	95.9 ± 7.1						
10^6	cnt-1	1/7	>420[b]						
10^7	cnt-1	3/7	>420[b]						
10^8	cnt-1	1/7	>420[b]						
10^9	cnt-1	2/7	>420[b]						

[a] Days after cerebral inoculation.
[b] Observed up to 420 days postinoculation.
[c] Observed up to 140 days postinoculation.
[d] Mouse for the sample in the left lane of 0.2% cpd-B at 63 dpi in Fig. 4A.
[e] Mouse for the sample in the right lane of 0.2% cpd-B at 63 dpi in Fig. 4A.
[f] Mouse for the sample of the rightmost lane of 0.2% cpd-B at 154 dpi in Fig. 4A.

Either variation in strain-specific PrP conformational structures or variation in microenvironments facilitating PrP conformational changes might be involved in the mechanism of prion strain-dependent efficacy. The results of this study showed that prions producing predominantly diglycosylated PrPres molecules were least sensitive or resistant to cpd-B treatment, which suggests that either the conformational structure responsible for PrPres or the diglycosylation moieties might affect the interaction of the compound with abnormal PrP molecules, although this inference must be examined further. The findings indicate that each class of antiprion compounds must be examined using various prion strains to learn more about prion strain dependency.

Even in the terminal stage of disease, both abnormal PrP deposition levels in the brain and infectivity levels in the brain were reduced in the mice treated with cpd-B compared to the nontreated control mice. It remains unclear why this gap occurs. One possibility is that the treated mice prematurely fell into the terminal stage because of accumulated cpd-B toxicity. This inference, however, does not seem to be correct, because the noninfected mice treated with 0.2% cpd-B feed for more than 1 year showed no clinical signs and appeared healthy. Another possibility is that neuronal cells in the brain might be more vulnerable to lower levels of abnormal PrP in the presence of cpd-B or that abnormal PrP bound with cpd-B might be more toxic to the neuronal cells in the brain. However, these inferences also seem to be unlikely, because the toxicity of PrP106-126 peptide amyloid, which is reminiscent of abnormal

PrP, in primary neuronal cell cultures is attenuated by the presence of cpd-B (unpublished data). Another possibility is that prion strains modified or selected from the original by the compound might multiply in the animals and cause the disease; this inference is supported by data showing that PrPres molecules with different glycoform patterns were detected in the treated mice. Further study, however, must provide evidence to support this inference. The findings indicate that life-threatening levels of either infectivity or abnormal PrP in the brain are not necessarily the same between treated animals and nontreated animals.

A large quantity of cpd-B was needed for efficacy in vivo; disease progression was not halted even though the treatment commenced immediately after the infection and continued to the terminal stage of disease. This limited effectiveness of cpd-B might be partly attributable to the pharmacological properties of its rapid washout from either the brain or the blood, because it is assumed that the compounds with better brain permeativity and longer retention in the brain might produce more beneficial results in prion-infected animals. In addition, some metabolic instability of the compound might be responsible for its limited effectiveness, especially the loss of efficacy during long-term administration. In fact, cpd-B is easily metabolized in the presence of mouse liver microsome extracts (unpublished data). Therefore, the pharmacokinetic parameters of this compound must be improved for better efficacy.

The effectiveness of cpd-B is dependent upon the timing and duration of administration; an earlier start of administration is

necessary to maximize beneficial results. Therefore, diagnostic measures in much earlier disease stages, especially presymptomatic stages, are vital to produce more beneficial outcomes. In addition, multidrug combination chemotherapy using several antiprion compounds with different actions might produce more beneficial results. This study suggests that cpd-B inhibits new formation of abnormal PrP but does not facilitate the degradation of already formed abnormal PrP, because a mixture of cpd-B with abnormal PrP did not modify the protease-resistant property of abnormal PrP. In addition, cpd-B itself has no activity to protect neuronal cells from neurotoxic insults aside from PrP amyloid (unpublished data), suggesting that cpd-B does not protect neuronal cells from neurodegenerative insults that are induced secondarily by abnormal PrP. Combinations of cpd-B with other compounds such as doxycycline, flupirtine, and simvastatin might be examples, but their efficacy must be evaluated. Doxycycline is a tetracycline antibiotic known to destabilize abnormal PrP (12). Flupirtine is a centrally acting nonopioid analgesic and protects neuronal cells from apoptotic cell death induced by toxic PrP106-126 peptide amyloid (29). It was used in clinical trials, where beneficial effects on cognitive functions in patients with CJD were proved (21). Simvastatin is a cholesterol-lowering drug known to prevent abnormal PrP formation in prion-infected cells, presumably by redistribution of normal PrP away from cholesterol-rich lipid rafts (13, 31). It prolongs survival times in prion-infected animals (16, 17).

Recently, long-term cerebroventricular administration of pentosan polysulfate (PPS), a clinical approach based on our preclinical study in rodent models of prion diseases (9), has been carried out in 26 patients with various types of diseases (27). Although its therapeutic efficacy remains to be confirmed, preliminary clinical experience indicates prolonged survival in some patients receiving long-term PPS (22, 27). Further prospective investigation of PPS administration is necessary to obtain high-quality evidence for its clinical benefits. However, this treatment has some weaknesses. One is the requirement for surgical implantation of a continuous infusion pump and an intraventricular catheter, which could become an obstacle to extension of clinical trials because of the potential risks of prion contamination in operating rooms and of operation instruments, although most developed countries now possess clearly defined and well established guidelines for safe surgical and anesthetic management of patients with prion diseases. Compared to such treatments, the treatments using orally available antiprion compounds are absolutely preferable and practical.

The compounds tested in the study were originally designed as therapeutic lead chemicals for the treatment of Alzheimer's disease. In fact, cpd-B and related chemicals are very effective in vitro in either inhibiting beta-amyloid formation or protecting neuronal cells from beta-amyloid toxicity; in addition, cpd-B has therapeutic efficacy in an Alzheimer's disease mouse model (unpublished data). Therefore, cpd-B is a therapeutic candidate not only for prion diseases but also for Alzheimer's disease. The search for and development of drugs for prion diseases reportedly do not interest pharmaceutical companies because of the limited number of patients, but the possible use of amyloidophilic chemicals as drug candidates for both prion

diseases and Alzheimer's disease might attract and accelerate the development of therapeutic drugs for prion diseases.

In conclusion, our findings related to the newly synthesized amyloidophilic chemical cpd-B are encouraging, but further improvement of its safety profiles and pharmacokinetic properties is necessary before clinical application can be considered. Moreover, additional problems exist with its prion strain-dependent effectiveness and with its reduced effectiveness if administered at later disease stages.

REFERENCES

1. Adjou, K. T., J. P. Deslys, R. Demaimay, and D. Dormont. 1997. Probing the dynamics of prion diseases with amphotericin B. Trends Microbiol. 5:27–31.
2. Bresjanac, M., L. M. Smid, T. D. Vovko, A. Petric, J. R. Barrio, and M. Popovic. 2003. Molecular-imaging probe 2-(1-[6-[(2-fluoroethyl)(methyl)-amino]-2-naphthyl]ethylidene)malononitrile labels prion plaques in vitro. J. Neurosci. 23:8029–8033.
3. Cai, L., R. B. Innis, and V. W. Pike. 2007. Radioligand development for PET imaging of beta-amyloid (Abeta)—current status. Curr. Med. Chem. 14:19–52.
4. Cashman, N. R., and B. Caughey. 2004. Prion diseases—close to effective therapy? Nat. Rev. Drug Discov. 3:874–884.
5. Caughey, B., and R. E. Race. 1992. Potent inhibition of scrapie-associated PrP accumulation by Congo red. J. Neurochem. 59:768–771.
6. Caughey, B., and G. J. Raymond. 1993. Sulfated polyanion inhibition of scrapie-associated PrP accumulation in cultured cells. J. Virol. 67:643–650.
7. Doh-ura, K., E. Mekada, K. Ogomori, and T. Iwaki. 2000. Enhanced CD9 expression in the mouse and human brains infected with transmissible spongiform encephalopathies. J. Neuropathol. Exp. Neurol. 59:774–785.
8. Doh-Ura, K., T. Iwaki, and B. Caughey. 2000. Lysosomotropic agents and cysteine protease inhibitors inhibit scrapie-associated prion protein accumulation. J. Virol. 74:4894–4897.
9. Doh-ura, K., K. Ishikawa, I. Murakami-Kubo, K. Sasaki, S. Mohri, R. Race, and T. Iwaki. 2004. Treatment of transmissible spongiform encephalopathy by intraventricular drug infusion in animal models. J. Virol. 78:4999–5006.
10. Doh-Ura, K., T. Kuge, M. Uomoto, K. Nishizawa, Y. Kawasaki, and M. Iha. 2007. Prophylactic effect of dietary seaweed fucoidan against enteral prion infection. Antimicrob. Agents Chemother. 51:2274–2277.
11. Fischer, M., T. Rulicke, A. Raeber, A. Sailer, M. Moser, B. Oesch, S. Brandner, A. Aguzzi, and C. Weissmann. 1996. Prion protein (PrP) with amino-proximal deletions restoring susceptibility of PrP knockout mice to scrapie. EMBO J. 15:1255–1264.
12. Forloni, G., S. Iussich, T. Awan, L. Colombo, N. Angeretti, L. Girola, I. Bertani, G. Poli, M. Caramelli, M. Grazia Bruzzone, L. Farina, L. Limido, G. Rossi, G. Giaccone, J. W. Ironside, O. Bugiani, M. Salmona, and F. Tagliavini. 2002. Tetracyclines affect prion infectivity. Proc. Natl. Acad. Sci. USA 99:10849–10854.
13. Gilch, S., C. Kehler, and H. M. Schatzl. 2006. The prion protein requires cholesterol for cell surface localization. Mol. Cell Neurosci. 31:346–353.
14. Ishikawa, K., K. Doh-ura, Y. Kudo, N. Nishida, I. Murakami-Kubo, Y. Ando, T. Sawada, and T. Iwaki. 2004. Amyloid imaging probes are useful for detection of prion plaques and treatment of transmissible spongiform encephalopathies. J. Gen. Virol. 85:1785–1790.
15. Ishikawa, K., Y. Kudo, N. Nishida, T. Suemoto, T. Sawada, T. Iwaki, and K. Doh-ura. 2006. Styrylbenzoazole derivatives for imaging of prion plaques and treatment of transmissible spongiform encephalopathies. J. Neurochem. 99:198–205.
16. Kempster, S., C. Bate, and A. Williams. 2007. Simvastatin treatment prolongs the survival of scrapie-infected mice. Neuroreport 18:479–482.
17. Mok, S. W., K. M. Thelen, C. Riemer, T. Bamme, S. Gultner, D. Lutjohann, and M. Baier. 2006. Simvastatin prolongs survival times in prion infections of the central nervous system. Biochem. Biophys. Res. Commun. 348:697–702.
18. Murakami-Kubo, I., K. Doh-Ura, K. Ishikawa, S. Kawatake, K. Sasaki, J.

Kira, S. Ohta, and T. Iwaki. 2004. Quinoline derivatives are therapeutic candidates for transmissible spongiform encephalopathies. J. Virol. **78:**1281–1288.

19. **Okamura, N., T. Suemoto, H. Shimadzu, M. Suzuki, T. Shiomitsu, H. Akatsu, T. Yamamoto, M. Staufenbiel, K. Yanai, H. Arai, H. Sasaki, Y. Kudo, and T. Sawada.** 2004. Styrylbenzoxazole derivatives for in vivo imaging of amyloid plaques in the brain. J. Neurosci. **24:**2535–2541.

20. **Okamura, N., T. Suemoto, S. Furumoto, M. Suzuki, H. Shimadzu, H. Akatsu, T. Yamamoto, H. Fujiwara, M. Nemoto, M. Maruyama, H. Arai, K. Yanai, T. Sawada, and Y. Kudo.** 2005. Quinoline and benzimidazole derivatives: candidate probes for in vivo imaging of tau pathology in Alzheimer's disease. J. Neurosci. **25:**10857–10862.

21. **Otto, M., L. Cepek, P. Ratzka, S. Doehlinger, I. Boekhoff, J. Wiltfang, E. Irle, G. Pergande, B. Ellers-Lenz, O. Windl, H. A. Kretzschmar, S. Poser, and H. Prange.** 2004. Efficacy of flupirtine on cognitive function in patients with CJD: a double-blind study. Neurology **62:**714–718.

22. **Parry, A., I. Baker, R. Stacey, and S. Wimalaratna.** 2007. Long term survival in a patient with variant Creutzfeldt-Jakob disease treated with intraventricular pentosan polysulphate. J. Neurol. Neurosurg. Psychiatry **78:**733–734.

23. **Prusiner, S. B., M. P. McKinley, K. A. Bowman, D. C. Bolton, P. E. Bendheim, D. F. Groth, and G. G. Glenner.** 1983. Scrapie prions aggregate to form amyloid-like birefringent rods. Cell **35:**349–358.

24. **Prusiner, S. B.** 1991. Molecular biology of prion diseases. Science **252:**1515–1522.

25. **Race, R. E., B. Caughey, K. Graham, D. Ernst, and B. Chesebro.** 1988. Analyses of frequency of infection, specific infectivity, and prion protein biosynthesis in scrapie-infected neuroblastoma cell clones. J. Virol. **62:**2845–2849.

26. **Race, R. E., S. A. Priola, R. A. Bessen, D. Ernst, J. Dockter, G. F. Rall, L. Mucke, B. Chesebro, and M. B. Oldstone.** 1995. Neuron-specific expression of a hamster prion protein minigene in transgenic mice induces susceptibility to hamster scrapie agent. Neuron **15:**1183–1191.

27. **Rainov, N. G., Y. Tsuboi, P. Krolak-Salmon, A. Vighetto, and K. Doh-Ura.** 2007. Experimental treatments for human transmissible spongiform encephalopathies: is there a role for pentosan polysulfate? Expert Opin. Biol. Ther. **7:**713–726.

28. **Sadowski, M., J. Pankiewicz, H. Scholtzova, J. Tsai, Y. Li, R. I. Carp, H. C. Meeker, P. Gambetti, M. Debnath, C. A. Mathis, L. Shao, W. B. Gan, W. E. Klunk, and T. Wisniewski.** 2004. Targeting prion amyloid deposits in vivo. J. Neuropathol. Exp. Neurol. **63:**775–784.

29. **Schroder, H. C., and W. E. Muller.** 2002. Neuroprotective effect of flupirtine in prion disease. Drugs Today **38:**49–58.

30. **Smid, L. M., T. D. Vovko, M. Popovic, A. Petric, V. Kepe, J. R. Barrio, G. Vidmar, and M. Bresjanac.** 2006. The 2,6-disubstituted naphthalene derivative FDDNP labeling reliably predicts Congo red birefringence of protein deposits in brain sections of selected human neurodegenerative diseases. Brain Pathol. **16:**124–130.

31. **Taraboulos, A., M. Scott, A. Semenov, D. Avrahami, L. Laszlo, and S. B. Prusiner.** 1995. Cholesterol depletion and modification of COOH-terminal targeting sequence of the prion protein inhibit formation of the scrapie isoform. J. Cell Biol. **129:**121–132.

32. **Trevitt, C. R., and J. Collinge.** 2006. A systematic review of prion therapeutics in experimental models. Brain **129:**2241–2265.

Impairment of Microglial Responses to Facial Nerve Axotomy in Cathepsin S–Deficient Mice

Hai Peng Hao,[1] Katsumi Doh-ura,[2] and Hiroshi Nakanishi[1]*

[1]Laboratory of Oral Aging Science, Faculty of Dental Sciences, Kyushu University, Fukuoka, Japan
[2]Department of Prion Research, Tohoku University, Sendai, Japan

Cathepsin S (CS) is a lysosomal/endosomal cysteine protease especially expressed in cells of a mononuclear lineage including microglia. To better understand the role of CS in microglia, we investigated microglial responses after a facial nerve axotomy in CS-deficient (CS−/−) and wild-type mice. Microglia in both groups accumulated in the facial motor nucleus following axotomy. However, the mean number of microglia in CS−/− mice on the axotomized side was significantly smaller than that in wild-type mice. Microglia were found to adhere to injured motoneurons in wild-type mice, whereas microglia abutted on injured motoneurons without spreading on their surface in CS−/− mice. At the same time, the axotomy-induced down-regulation of tenasin-R, an antiadhesive perineuronal net for microglia, was partially abrogated in CS−/− mice. Primary cultured microglia prepared from CS−/− mice showed that CS deficiency caused significant suppression of migration and transmigration of microglia. In CS−/− mice, impaired recruitments of circulating monocytes and T lymphocytes and reduced expression of the class II major compatibility complex on the axotomized side were observed. Interestingly, cathepsin B, a typical lysosomal cysteine protease, was markedly expressed on the axotomized side in CS−/− but not in wild-type microglia. Finally, we compared axotomy-induced neuronal death in the two groups and found that the percentage of motoneurons that survived in CS−/− mice was significantly smaller than that in wild-type mice. The present study strongly suggests that CS plays a role in the migration and activation of microglia to protect facial motoneurons against axotomy-induced injury. © 2007 Wiley-Liss, Inc.

Key words: cathepsin S–deficient mice; facial nerve axotomy; microglia; cathepsin B; transmigration; motoneuron survival

Cathepsin S (CS) is a member of the lysosomal cysteine protease family, which is preferentially expressed in cells of mononuclear-phagocytic origin including microglia (Petanceska et al., 1996). In response to lipopolysaccharide (LPS), a substantial increase in the activity of CS secreted from both macrophages and microglia is observed (Petanceska et al., 1996). CS retains its proteolytic activity even after prolonged exposure to a neutral pH (Bromme et al., 1989, 1993). CS has been reported to degrade several extracellular matrix (ECM) molecules including fibrillar collagen, elasin, laminin, fibronectin, and heparan sulfate proteoglycans at a neutral pH (Liuzzo et al., 1999). CS-deficient (CS−/−) monocytic cells showed impaired subendothelial basement membrane transmigration (Sukhova et al., 2003). Furthermore, CS plays a pivotal role in antigen presentation because this enzyme is an essential requirement for invariant chain processing in antigen-presenting cells including dendritic cells and microglia (Nakagawa et al., 1999; Shi et al., 1999; Nishioku et al., 2002) without affecting expression of the class II major compatibility complex (MHC II). The cell type–specific localization and enzymatic nature of CS both contrast sharply with other types of lysosomal cysteine proteases including cathepsin B (CB). CB is expressed in almost all cell types and is also secreted from microglia as the heavy chain form in addition to the proform on stimulation with LPS (Ryan et al., 1995). However, it is well known that CB is irreversibly inactivated at a neutral pH. In addition to playing a role in intracellular proteolysis, CS secreted by microglia and monocytic cells may also play a role in extracellular proteolysis among different types of lysosomal cysteine proteases. We may therefore speculate that CS plays a specific role in the reactions of microglia and monocytic cells including migration, adhesion, transmigration, and antigen presentation (Nakanishi, 2003).

It is well known that microglia exhibit a series of reactions after facial nerve axotomy (Ravich et al., 1999; Moran and Graeber, 2004). Following axotomy, micro-

glia are rapidly activated and then are transformed into a deramified form; thereafter, they proliferate, adhere to injured motoneurons, and spread on their surfaces. Monocytic cells recruited to the brain parenchyma through the cerebral vasculature and the leptomeninges also adhere to injured motoneurons (Priller et al., 2001; Bechmann et al., 2005). Although the precise pathological significance of the perineuronal satellite position of microglia remains unclear, the adhesion of microglia to injured motoneurons may be essential for neuronal survival, thus leading to axonal regeneration. Activated microglia may displace synaptic input, a phenomenon known as synaptic stripping (Blinzinger and Kreutzberg, 1968). The tight adhesion of microglia could enhance uptake of diffusible molecules leaked from injured motoneurons and trans-synaptic uptake of their breakdown products as well as of pathogens (Ravich et al., 1999; Kalla et al., 2001). On the other hand, microglia express MHC II and costimulatory factors (Streit et al., 1989) and interact with T lymphocytes recruited to the axotomized facial motor nucleus (Ravich et al., 1998). Therefore, microglia may also play a pivotal role in immune surveillance as an antigen-presenting cells in the axotomized facial motor nucleus. Following a facial nerve axotomy, there was marked up-regulation in microglia of CS and cystatin C (CysC), the latter an endogenous inhibitor for cysteine proteases (Miyake et al., 1996; Uwabe et al., 1997). Up-regulation of CS may be closely associated with microglial responses to a facial nerve axotomy because ECM degradation is required for the rapid migration, adhesion, and transmigration of microglia and monocytic cells. Moreover, CS is essential for antigen presentation by microglia (Nishioku et al., 2002). However, no report has previously elucidated the precise function of CS in microglial reactions to a facial nerve axotomy.

In the present study, we examined the effects of CS deficiency on microglial reactions to a facial nerve axotomy and facial motoneuron survival. We found that CS deficiency markedly impaired cellular responses of microglia to a facial nerve axotomy, thereby promoting axotomy-induced facial motoneuron death.

MATERIALS AND METHODS

Animals

Heterozygous mice (CS+/−) mice on a DBA background were provided by Dr. William H. Brissette (Central Research Division, Pfizer Inc., Groton, CT; Nakagawa et al., 1999) and maintained under specific pathogen-free conditions at Kyushu University Faculty of Dentistry. Selection of CS−/− mice from littermates obtained by heterozygous coupling was performed by template genomic DNA isolated from tail biopsies examined to detect the neomycin cassette by neoexon 6− and exon 5−specific PCR with primers of cs6-1 (5'-TAC-CCGCTTCCATTGCTCAG-3'), cs6-2 (5'-TCTTTCAGG-GCATCTTCGTC-3'), cs5-1 (5'-GGTTCTTGTGGTGCC-TGTTG-3'), and cs5-2 (5'-GTGGCTTTGTAGGGATGGA-3').

Surgical Procedures

All operations were performed under anesthesia with pentobarbital (40 mg/kg intraperitoneally, i.p.). The right facial nerves of 6-week-old CS−/− and wild-type mice were transected approximately 1 mm at the stylomastoid foramen. Failure of a mouse to move the whiskers on the right side of the face following recovery from anesthesia was considered verification of the success of the axotomy.

Immunohistochemistry

Detailed indirect fluorescent immunohistochemistry has been previously described (Nakanishi et al., 2001; Shimizu et al., 2005). Briefly, 2, 4, 7, 14, 30, and 50 days after axotomy, the specimens were obtained from CS−/− and wild-type mice (n = 4 each), which were anesthetized with sodium pentobarbital (40 mg/kg, i.p.) and killed by intracardiac perfusion with isotonic saline, followed by a chilled fixative consisting of 4% paraformaldehyde (PFA) in 0.2M phosphate-buffered saline (pH 7.4). After perfusion, the brain was removed, further fixed by immersion in the same fixative overnight at 4°C, and then immersed in 20% sucrose (pH 7.4) for 24 hr at 4°C. Floating parasagittal sections (30 μm thick) of the brain stem were prepared by a cryostat (CM1850 Leica, Nusloch, Germany) and stained with rabbit polyclonal anti-ionized calcium-binding adaptor molecule 1 (Iba1) antibody (1:500; Wako Pure Chemical Industries, Ltd., Osaka, Japan), OX6 (1:100; Serotec, Oxford, UK), mouse monoclonal anti-tenascin R (TNR) antibody (1:100; R&D Systems Inc., Minneapolis, MN), or rabbit polyclonal anti-choline acetyltransferase (ChAT, 1:500; Chemicon International) for 3 days at 4°C. After washing with phosphate-buffered saline (PBS), the sections were stained with biotinylated antirabbit, antimouse, or antigoat IgG (Vector Laboratories, Burlingame, CA) overnight. After washing with PBS, the sections were stained with ABC reagent (Vector Laboratories, Burlingame, CA) or Alexa 488 0.5% streptavidin (Molecular Probes, Eugene, OR). The sections that reacted with ABC reagent were developed with diaminobenzidine, dehydrated in alcohol and xylene, and then mounted. The sections that reacted with Alexa 488 streptavidin were mounted with Vectashield antifading medium (Vector Laboratories).

For double staining, floating parasagittal sections (30 μm thick) of the brain stem were incubated with goat polyclonal anti-CS antibody (1:300; Santa Cruz Biotechnology, Inc., Santa Cruz, CA), rabbit polyclonal anti-CB (1:200; Upstate, Lake Placid, NY), anti-ChAT (1:500), rabbit polyclonal anti-CysC (1:300; Upstate), or mouse monoclonal anti-CD3 (1:500; BD Biosciences, Bedford, MA) antibody for 3 days at 4°C. After washing with PBS, the sections were treated with 0.5% antirabbit or antigoat IgG conjugated with Cy3 (Jackson ImmunoResearch Laboratories, Inc., West Grove, PA) for 2 hr at room temperature. They were then further treated with anti-Iba1 antibody (1:500) or F4/80 (1:50; Serotec, Oxford, UK) for 3 days at 4°C. After washing with PBS, the sections were treated with 0.5% antirabbit IgG or antimouse IgG conjugated with Alexa 488 (Molecular Probes, Eugene, OR) for 2 hr at room temperature. The sections incubated with anti-ChAT antibody were also treated with 0.5% anti-

rabbit IgG conjugated with Alexa 488 (Molecular Probes) for 2 hr at room temperature. The sections were treated with mouse monoclonal anti-GFAP antibody (Sigma, St. Louis, MO) for 3 days at 4°C and then were further incubated with 0.5% antimouse IgG conjugated with Cy3 (Jackson Immunoresearch Laboratories). The sections were mounted in the Vectashield antifading medium (Vector Laboratories, Burlingame, CA) and examined by a confocal laser scanning microscope (CLSM; LSM510META, Carl Zeiss, Jena, Germany).

Evaluation of Microglial Morphology

To quantitatively describe the differences in microglial morphology between CS−/− and wild-type mice after axotomy, we adopted a transformation index (TI), which was calculated by the equation, [perimeter of cell $(\mu M)]^2/4\pi$ [cell area (μm^2)] (Fujita et al., 1996). Five sections (30 μm thick) stained with anti-Iba1 antibody were randomly selected from each of the CS−/− and wild-type mice (n = 3 each). Images of individual sections, photographed with a conventional CCD camera with a 20X objective (numerical aperture = 0.75), were analyzed with an image analyzer to determine their perimeters and areas. The TI was calculated for the axotomized and control sides of the CS−/− and wild-type mice 2, 4, and 7 days after axotomy.

Electrophoresis and Immunoblotting

The supernatant fractions of the facial nuclei were prepared from CS−/− (n = 3) and wild-type (n = 3) mice 7 days after axotomy, in which the mice were anesthetized with sodium pentobarbital (40 mg/kg, i.p.) and killed by intracardiac perfusion with isotonic saline. Each homogenate was electrophoresed in 7%–12% sodium dodecyl sulfate (SDS)–polyacrylamide gels. Proteins on SDS gels were transferred electrophoretically to nitrocellulose membranes. The protein transfers were blocked in 5% skim milk for 1 hr at room temperature under gentle agitation. The blots were then incubated with anti-CS (1:1,000), anti-CB (1:1,000), anti-CysC (1:1,000), anti-TNR (1:500), or antiactin (1:1,000, Santa Cruz Biotechnology, Santa Cruz, Santa Cruz, CA) antibodies overnight at 4°C under gentle agitation. After washing, the blots were incubated with 0.02% horseradish peroxidase (HRP)–labeled donkey antirabbit or antimouse IgG (Amersham). Subsequently, the membrane-bound, HRP-labeled antibodies were detected by an enhanced chemiluminescence detection system (ECL kit, Amersham) with an image analyzer LAS-1000 (Fuji Photo Film, Tokyo, Japan). The protein bands were then scanned and analyzed densitometrically.

mRNA Extraction and Reverse Transcriptase (RT)-PCR

mRNA was prepared from the facial nuclei from CS−/− (n = 3) and wild-type (n = 3) mice 7 days after axotomy, and then the mice were anesthetized with sodium pentobarbital (40 mg/kg, i.p.) using a QuickPrep micro mRNA purification kit (Amersham Oharmacia Biotech, England, UK), and the first cDNA was synthesized using SuperScript II (Invitrogen, Carlsbad, CA). For PCR, the cDNA was amplified by Tag DNA polymerase (Invitrogen). Reverse transcription was

performed at 60°C for 15 min in 0.5 mg of mRNA. PCR amplification was performed in the DNA amplifier cycle (Techne Duxford, UK) after an initial cycle at 94°C for 2 min for 40 cycles of 1 min at 94°C and 1.5 min at 60°C. The RT-PCR products were run on 2% agarose gel and stained with ethidium bromide. Glyceroldehydes-3-phosphate dehydrogenase (GAPDH)–specific primers were used as a control with 1 mL of template cDNA. Primers for CS were 5′-GAC-ATTGCCTGACACTGTGG-3′ and 5′-CATGTTCACATT-GCCCGTA-3′, primers for CB were 5′-CTCTGGAGCAT-GGAGCTTCT-3′ and 5′-ATGCCACAGTGGTTTTCTCC-3′, primers for CysC were 5′-AGCGAGTACAAC-AAGGG-CAG-3′ and 5′-CAAGAAGAGTGAAGCCAGGG-3′, and primers for GAPDH were 5′-TCCACCACCCTGTTGCTGTA-3′ and 5′-ACCACAGTCCATGCCATCAC-3′.

Microglial Culture

Microglia were isolated from mixed primary cell cultures from whole-brain samples of 3-day-old CS−/− and wild-type mice according to methods described previously (Nishioku et al., 2002). Eagle's minimal essential medium (MEM) containing 10% fetal calf serum, penicillin G (40 U/mL), and streptomycin (50 mg/mL) was used for culture medium. After 10–14 days in culture, floating cells and weakly attached cells in the mixed glial cell layer were isolated by shaking of the flask. The resulting cell suspension was transferred to a petri dish (Falcon 1001, Lincoln Park, NJ) and allowed to adhere at 37°C. Unattached cells were removed after 30 min, and microglia were isolated as strongly adhering cells. The microglia were more than 96% pure, as determined by the immunostaining of Iba1.

Cell Proliferation Assay

Cell viability was measured 24 hr after treatment with macrophage colony-stimulating factor (M-CSF, R&D Systems Inc., Minneapolis, MN) or granulocyte macrophage colony-stimulating factor (GM-CSF, Genzyme, Cambridge, MA) by WST-8 conversion to water-soluble formazan by mitochondrial dehydrogenase (Cell Counting Kit-8, Dojindo, Kumamoto, Japan). Briefly, WST-8 was added to the culture medium of primary cultured microglia prepared from CS−/− and wild-type mice growing in serum-free medium and incubated at 37°C for 4 hr. The supernatant was transferred to 96-well dishes and then was quantitated using a plate reader at 450 nm.

Cell Migration Assay

Cell migration of microglia was assessed using the Boyden chamber. Polycarbonate filters with pores of 3 μM precoated with fibronectin (Becton Dickison Labware, Bedford, MA) were used. Five hundred microliters of microglial cell suspension in serum-free MEM containing 0.3% bovine serum albumin prepared from CS−/− and wild-type mice was plated on cell inserts at a cell density of 10^5. All inserts were dipped into lower wells contained 750 μL of serum-free MEM containing 100 μM ATP as a chemical attractant. The plates were incubated at 37°C in a 10% CO_2 atmosphere for 6 and 24 hr. Cells remaining on the upper surface of the

membrane were removed by wiping, and migrated cells were fixed with 4% PFA and subjected to Diff-Quik stain (Sysmex Corp., Kobe, Japan). Microglia that migrated to the lower surface of the membrane were manually counted in eight randomly chosen fields under a microscope with a 20× objective. Each assay was performed in triplicate.

Cell Transmigration Assay

Cell transmigration of microglia was assessed using a Matrigel chamber. Polycarbonate filters with pores of 8 μM precoated with Matrigel basement membrane matrix (BD Biosciences) were used. Five hundred microliters of microglial cell suspension in serum-free MEM containing 0.3% bovine serum albumin prepared from CS−/− and wild-type mice was plated on cell inserts at a cell density of 2×10^5. All inserts were dipped into lower wells contained 750 μL of serum-free MEM containing 100 μM ATP as a chemical attractant. In some experiments using primary culture microglia prepared from wild-type mice, benzyloxycarbonyl-Phe-Leu-α-keto-β-aldehyde (Z-FL-COCHO; Calbiochem, San Diego, CA), a specific inhibitor of CS, was added to serum-free MEM. Plates were incubated at 37°C in 10% CO_2 atmosphere for 24 hr. Cells remaining on the upper surface of the membrane were removed by wiping and the transmigrated cells were fixed with 4% PFA and subjected to Diff-Quik stain (Sysmex Corp.). The number of microglia that transmigrated to the lower surface of the membrane was manually counted in eight randomly chosen fields under a microscope with a 20× objective. Each assay was performed in triplicate.

Intrasplenic Injection of 6-Carboxylfluorescein Diacetate (CFDA)

CS−/− and wild-type mice (n = 3 each) were anesthetized with sodium pentobarbital (40 mg/kg, i.p.). A 0.5 cm incision was made on the left lateral abdomen. After preparing the surface of the spleen, 100 μL of a solution containing 2% of the long-lasting fluorescent tracker CFDA (Molecular Probes) in 0.1M PB was slowly injected. Twenty-four hours after the intrasplenic injection of CFDA, the right-side facial nerves were axotomized.

Quantitative Analysis of Facial Motoneurons

The optical dissector method using CLSM images (Jinno et al., 1998; Shimizu et al., 2005) was used to measure the numerical density of facial motoneurons. Five 30-μm-thick serial sections of a facial motor nucleus stained with anti-ChAT antibody were prepared from CS−/− and wild-type mice (n = 3 each) that had been subjected to facial nerve axotomy 4, 7, 30, and 50 days earlier. Images of individual sections were taken as a stack at 1-μm step size along the z direction with a 20× objective by a CLSM (LSM510MET). Data were transferred to a Power Mac G4 computer (Apple) and then analyzed using NIH Image software (version 1.62). Antibodies from the surface sufficiently permeated the full thickness of both CS−/− and wild-type mice brain sections. The number of ChAT-immunoreactive cells in each of five serial sections of a facial motor nucleus was summed. The data were averaged for each animal and then for each group. The calculated
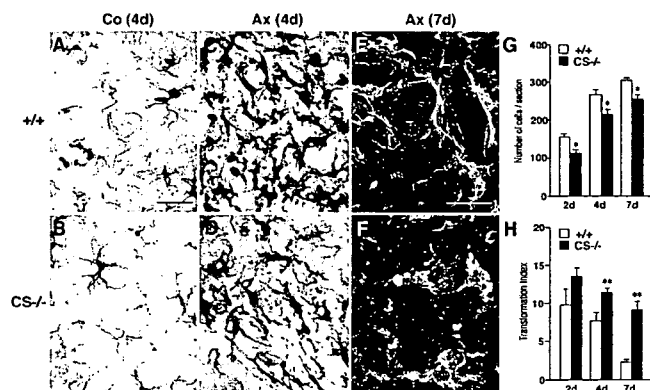

Fig. 1. Microglial responses following facial nerve axotomy in CS−/− and wild-type mice. **A:** Iba1-stained microglia in facial motor nuclei on control side (Co) of wild-type mice 4 days after axotomy. Scale bar = 50 μm. **B:** Iba1-stained microglia in facial motor nuclei on Co side of CS−/− mice 4 days after axotomy. **C:** Iba1-stained microglia in facial motor nuclei on axotomized side (Ax) of wild-type mice 4 days after axotomy. **D:** Iba1-stained microglia in facial motor nuclei on Ax side of CS−/− mice 4 days after axotomy. **E:** High-resolution CLSM images of Iba1-stained microglia on the axotomized side of facial motor nuclei of wild-type mice 7 days after axotomy. Scale bar = 25 μm. **F:** High-resolution CLSM images of Iba1-stained microglia on the axotomized side of facial motor nuclei of CS−/− mice 7 days after axotomy. Each section was taken as a stack at 1-μm step size along the z direction with a 100× objective by a CLSM. **G:** Number of microglia accumulated in axotomized facial motor nuclei of wild-type and CS−/− mice (open and solid columns, respectively) 2, 4, and 7 days after axotomy. Each column and bar represents the mean ± SD of three experiments (*significant difference at $P < 0.05$). **H:** TI of microglia accumulated in the axotomized facial motor nuclei of wild-type and CS−/− mice (open and solid columns, respectively) 2, 4, and 7 days after axotomy. TI was calculated by the equation [perimeter of cell (μM)]² /4π [cell area (μm²)].

numerical profile densities of the groups were compared using the Student t test.

Statistical Analysis

Data are expressed as means ± SDs. The statistical analyses were performed using the Student t test.

RESULTS

Alterations of Microglial Responses to Facial Nerve Axotomy in CS−/− Mice

No obvious abnormality in CS−/− mice compared to wild-type mice was noticed. We first focused on the microglial responses to the facial nerve axotomy. Following axotomy, microglia on the axotomized side of mice in both groups showed activated cell morphology characterized by a large cell body with thick processes. On the other hand, microglia on the control side maintained a normal ramified morphology (Fig. 1A,B). Four days after axotomy, there was a marked difference between the two groups in the morphology of microglia on the axotomized side. In wild-type mice, microglia had relatively small

cell bodies with thin processes (Fig. 1C). In contrast, in CS−/− mice most microglia still had rather large cell bodies with short processes (Fig. 1D). These morphological differences in microglia became more prominent 7 days after axotomy. CLSM images clearly showed that microglia spread on the surfaces of injured motoneurons, forming a thin continuum rimlike structure, in the wild-type mice (Fig. 1E). In CS−/− mice, most microglia still had rather large cell bodies with short processes and abutted injured motoneurons without spreading on their surface (Fig. 1F).

We further quantitated the number and morphological transformation of microglia on the axotomized side of the facial motor nuclei of both groups. As shown in Figure 1G, the mean number of microglia that had accumulated on the axotomized side of the facial motor nuclei of CS−/− mice was significantly smaller than that of wild-type mice. The morphological transformation of microglia after axotomy was also quantitated as a TI using the equation [perimeter of cell $(\mu M)]^2/4\pi$ [cell area (μm^2)]. The mean TI of CS−/− mice was significantly larger than that of wild-type mice 4 days after axotomy (Fig. 1H).

Reduced TNR Down-Regulation in Facial Motor Nuclei of CS−/− Mice following Axotomy

Next, we tried to determine why the CS−/− microglia failed to spread on the surfaces of facial motoneurons after axotomy. It has been reported that TNR that presents in the perineuronal net of motoneurons acts as antiadhesive for activated microglia (Angelov et al., 1998). Furthermore, expression of TNR was markedly down-regulated after axotomy. Therefore, it is tempting to speculate that insufficient down-regulation of TNR in CS−/− mice may prevent microglia from spreading onto the surfaces of axotomized facial motoneurons. To determine if this were true, we examined the level of TNR in the facial motor nuclei of CS−/− and wild-type mice after axotomy. In both groups, the total amount of TNR significantly decreased on the axotomized side (Fig. 2A). However, there was a greater decrease in the amount of TNR in the CS−/− mice than in the wild-type mice. This was substantiated with immunostaining with anti-TNR antibody (Fig. 2B). Although the immunoreactivity for TNR diffusely spread throughout a facial motor nucleus, the most intense immunoreactivity was found on the surface of cell somata of motoneurons in both groups. Seven days after axotomy, there was a marked reduction in the immunoreactivity for TNR on the axotomized side of the facial motor nuclei of wild-type mice. In contrast, only a moderate reduction in immunoreactivity for TNR was found in the CS−/− mice.

Effects of CS Deficiency on ATP-Induced Migration/Transmigration and GM-CSF-Induced Proliferation of Primary Cultured Microglia

Rapid accumulation of microglia occurred in the facial nuclei after axotomy mainly because of the prolifer-
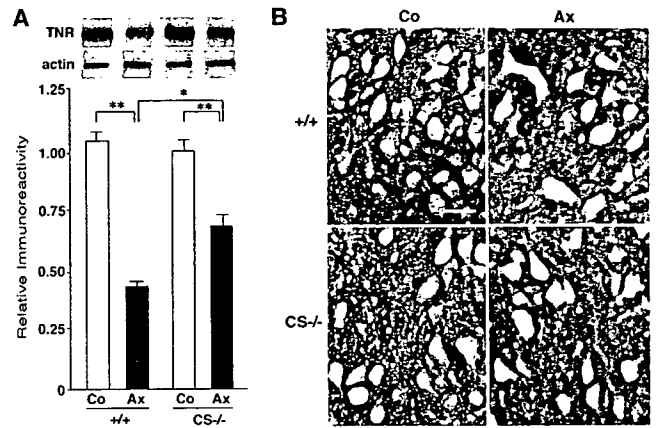

Fig. 2. Reduction in axotomy-induced down-regulation of TNR in facial motor nuclei of CS−/− mice 7 days after axotomy. A: Immunoblot analyses of TNR levels on the control (Co) and axotomized (Ax) sides (open and solid columns, respectively) of facial motor nuclei of CS−/− and wild-type mice. Mean relative immunoreactivity of TNR band was determined using expression of actin as an internal control. Each column and bar represents the mean ± SD of three experiments (**significant difference at $P < 0.01$). B: Immunohistochemical staining of TNR on Co and Ax sides of facial motor nuclei of CS−/− and wild-type mice. A marked reduction in the immunoreactivity for TNR was observed in axotomized facial motor nuclei of wild-type mice but not in CS−/− mice. Scale bar = 75 μm.

ation and migration of microglia as a result of cellular activation (Ravich et al., 1999; Moran and Graeber, 2004). There is increasing evidence that in addition to the contributions made by proliferation and migration, recruitment of monocytic cells through the cerebral vasculature and the leptomeninges also adds to the increased number of microglia on the axotomized side of the facial motor nucleus (Priller et al., 2001; Bechmann et al., 2005). Thus, we next compared the proliferative, migratory, and proliferative abilities of primary cultured microglia prepared from CS−/− and wild-type mice because there was a significant reduction in the number of microglia on the axotomized side of the facial motor nuclei of CS−/− mice.

M-CSF is a major mitogen for microglia in the axotomized facial nucleus (Raivichet al., 1994). Furthermore, an experiment involving GM-CSF binding in axotomized facial nuclei showed GM-CSF to be a plausible mitogen (Ravich et al., 1991). We thus used both M-SCF and GM-CSF as mitogens to examine the effect of CS deficiency on cell-proliferating ability. As shown in Figure 3A, there was no significant difference between the two groups in the cell-proliferating ability of microglia after stimulation with either M-CSF or GM-CSF. We next conducted ATP-induced cell migration assay using a Boyden chamber. The wild-type and CS−/− microglia that migrated to the opposite side of the fibronectin-coated membrane after treatment with ATP were counted. As shown in Figure 3B, the mean number of migrated CS−/− microglia 24 hr after treatment with
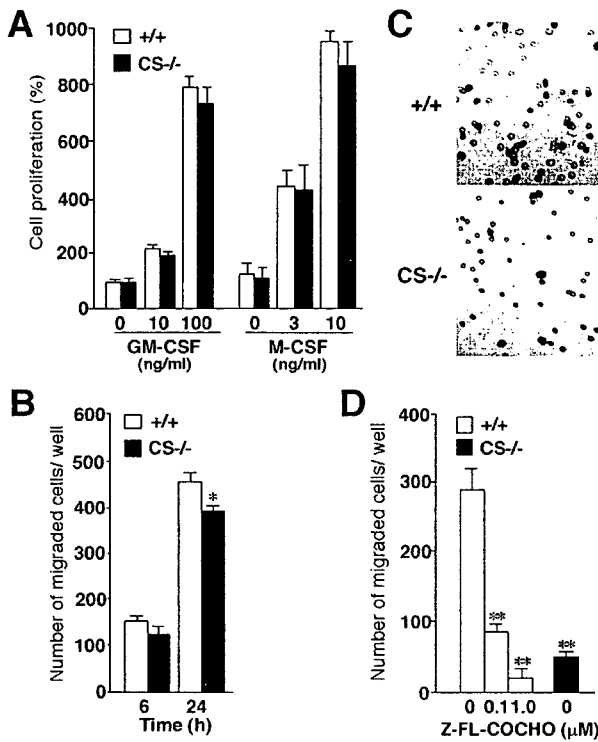
Fig. 3. Effects of CS deficiency on proliferation, migration, and transmigration of primary cultured microglia. A: Mean survival ratio of CS−/− and wild-type microglia 24 hr after treatment with M-CSF or GM-CSF. Each column and bar represents the mean ± SD of three experiments. B: ATP-induced migration of primary cultured microglia prepared from CS−/− and wild-type mice detected by the Boyden chamber. Mean number of CS−/− and wild-type microglia that migrated to the opposite side of a fibronectin-coated membrane, assessed by a Boyden chamber 6 and 24 hr after treatment with ATP (100 μM). Each column and bar represents the mean ± SD of three experiments (*significantly different from the wild-type microglia at $P < 0.05$). C, D: ATP-induced transmigration of primary cultured microglia prepared from CS−/− and wild-type mice, detected by a Matrigel invasion chamber. C: CS−/− and wild-type microglia that transmigrated to the opposite side of the Matrigel basement membrane matrix. Scale bar = 85 μm. D: Mean number of CS−/− and wild-type microglia as well as wild-type microglia treated with Z-FL-COCHO that transmigrated to opposite side of the Matrigel basement membrane matrix 24 hr after treatment with ATP (100 μM). Each column and bar represents the mean ± SD of three experiments (**significantly different from the wild-type control at $P < 0.01$).

ATP (100 μM) was slightly but significantly smaller than that of migrated wild-type microglia. We further conducted an ATP-induced cell transmigration assay using a Matrigel invasion chamber. The mean number of CS−/− microglia transmigrated through the Matrigel basement membrane matrix 24 hr after treatment with ATP (100 μM) was significantly lower than that of wild-type microglia (Fig. 2C,D). Furthermore, a specific inhibitor of CS, Z-FL-COCHO, significantly inhibited the transmigration of wild-type microglia through the Matrigel basement membrane matrix in a dose-dependent manner (Fig. 3D).
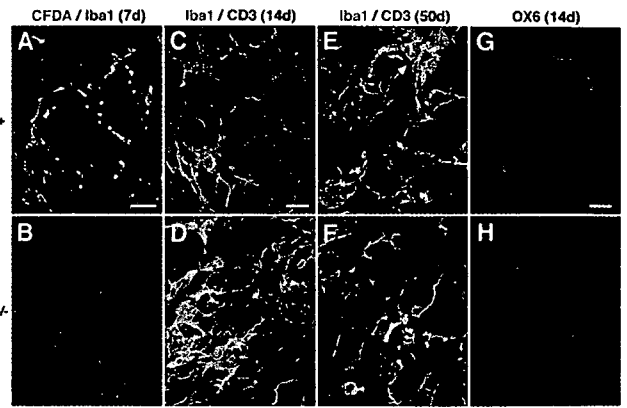

Fig. 4. Impairment of axotomy-induced recruitment of CFDA-labeled splenocytes and T lymphocytes in the facial motor nuclei of CS−/− mice. A: Immunofluorescent CLSM image of facial motor nuclei of wild-type mice 7 days after axotomy showing that the CFDA-labeled cells (green) are visible on the axotomized side. Scale bar = 35 μ. B: Immunofluorescent CLSM image of facial motor nuclei of CS−/− mice 7 days after axotomy showing that the CFDA-labeled cells (green) are not visible on the axotomized side. The CFDA-labeled cells corresponded well with microglia (red), which spread on the surface of injured facial motoneurons. C: CLSM image of infiltrated CD3-positive T lymphocytes (red) and Iba1-positive microglia (green) in facial motor nuclei of wild-type mice 14 days after axotomy. Scale bar = 40 μm. D: CLSM image of infiltrated CD3-positive T lymphocytes (red) and Iba1-positive microglia (green) in facial motor nuclei of CS−/− mice 14 days after axotomy. E: CLSM image of infiltrated CD3-positive T lymphocytes (red) and Iba1-positive microglia (green) in facial motor nuclei of wild-type mice 50 days after axotomy. Scale bar = 40 μm. F: CLSM image of infiltrated CD3-positive T lymphocytes (red) and Iba1-positive microglia (green) in facial motor nuclei of CS−/− mice 50 days after axotomy. G: CLSM images of immunoreactivity for MHC II-positive cells in facial motor nuclei of wild-type mice 14 days after axotomy. Scale bar = 30 μm. H: CLSM images of immunoreactivity for MHC II-positive cells in facial motor nuclei of CS−/− mice 14 days after axotomy.

Z-FL-COCHO did not have a significant cytotoxic effect on primary cultured microglia in the concentration range used in this study (data not shown).

Impaired Recruitment of Monocytic Cells and T Lymphocytes and Reduced MHC II Expression in Facial Motor Nuclei of CS−/− Mice after Axotomy

To further evaluate the effects of CS deficiency on cell transmigration, we examined the recruitment of monocytic cells and T lymphocytes into facial motor nuclei after axotomy. Seven days after axotomy, CFDA-fluorescent granules were detected on the axotomized side of the facial motor nuclei of intrasplenic CFDA-injected wild-type mice. These CFDA fluorescent granules were found to localize in 13% ± 3% of the Iba1-positive microglia (Fig. 4A). In contrast, we could not detect any CFDA fluorescent granules in the facial motor nuclei of CFDA-injected CS−/− mice (Fig. 4B). These obser-

vations indicated that approximately 10% of the Iba1-positive cells that accumulated on the axotomized side thus originated from circulating monocytic cells and that the CS deficiency significantly suppressed the recruitment of these monocytic cells.

We also examined recruitment of T lymphocytes in the facial motor nuclei 14 and 50 days after axotomy. In wild-type mice, CD3-positive T lymphocytes were detected to infiltrate the axotomized side (Fig. 4C,E). The mean number of CD3-positive cells per section 14 and 50 days after axotomy was approximately 4 and 12 cells/section, respectively. Fifty days after axotomy, the aggregated microglia were frequently surrounded by infiltrated CD3-positive T lymphocytes (Fig. 3E, arrow). In contrast, no CD3-positive cells were detected in the facial motor nuclei following axotomy (Fig. 4D,F).

We next examined the expression of MHC II because interactions with T lymphocytes are required for the induction of MHC II in antigen-presenting cells. As shown in Figure 4G, immunoreactivity for MHC II was observed in microglia-like cells as well as in perivascular-like cells in the facial motor nuclei of wild-type mice 14 days after axotomy. In contrast, only MHC II–positive perivascular-like cells were observed on the axotomized side of CS−/− mice (Fig. 4H).

Differential Axotomy-Induced Changes in CS, CB, and CysC Levels in CS−/− and Wild-Type Mice

We next measured the levels of CS, CB, and CysC, an endogenous cysteine protease inhibitor, at both the mRNA and protein levels in the facial motor nuclei of mice from both groups after axotomy. In wild-type mice, the mean levels of CS mRNA and CS protein (28-kDa active form) in the facial motor nucleus significantly increased after axotomy (Fig. 5A,B,E). Immunoblot analysis showed that under reducing conditions, using a CB-specific antibody, there were two mature forms of CB: a 29-kDa single-chain species and a 26-kDa heavy-chain species. Mean levels of CB mRNA and CB protein (29-kDa single-chain form) the facial motor nuclei of wild-type mice were not significantly changed after axotomy, whereas those of CS−/− mice significantly increased after axotomy (Fig. 5A,C,F). In contrast, mean levels of CysC mRNA and CysC protein (14 kDa) in the facial motor nuclei of CS−/− mice were significantly smaller than those of wild-type mice. After axotomy, mean levels of CysC mRNA and CysC protein (14 kDa) in the facial motor nuclei of mice in both groups significantly increased (Fig. 5A,D,G).

Localization of CS, CB, and CysC in the Facial Motor Nucleus after Facial Nerve Transection

Indirect immunofluorescent staining was used to further elucidate how cellular localization of CS, CB, and CysC increased after axotomy. It was found that CS localized in activated microglia that spread on the surfaces of injured motoneurons in wild-type mice (Fig. 6A). In contrast, immunoreactivity for CS was barely detectable in
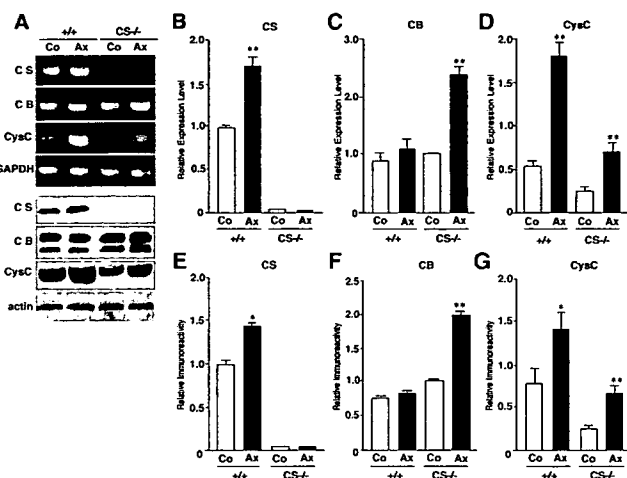

Fig. 5. Changes in CS, CB, and CysC levels in facial motor nuclei of CS−/− and wild-type mice 7 days after axotomy. A: Immunoblot and RT-PCR analyses of CS, CB, and CysC on control (Co) and axotomized (Ax) sides of facial motor nuclei of CS−/− and wild-type mice. B: Mean relative mRNA expression of CS, determined using expression of GAPDH as an internal control, on Co and Ax sides (open and solid columns, respectively) of facial motor nuclei of CS−/− and wild-type mice. C: Mean relative mRNA expression of CB, determined using expression of GAPDH as an internal control, on Co and Ax sides (open and solid columns, respectively) of facial motor nuclei of CS−/− and wild-type mice. D: Mean relative mRNA expression of CysC, determined using expression of GAPDH as an internal control, on Co and Ax sides (open and solid columns, respectively) of facial motor nuclei of CS−/− and wild-type mice. Each column and bar represents the mean ± SD of three experiments (**significantly different from the value in Co at $P < 0.01$). E: Mean level of CS protein, determined using expression of actin as an internal control, on Co and Ax sides (open and solid columns, respectively) of facial motor nuclei of CS−/− and wild-type mice. F: Mean level of CB protein, determined using expression of actin as an internal control, on Co and Ax sides (open and solid columns, respectively) of facial motor nuclei of CS−/− and wild-type mice. G: Mean level of CysC protein, determined using expression of actin as an internal control, on Co and Ax sides (open and solid columns, respectively) of facial motor nuclei of CS−/− and wild-type mice. Each column and bar represents the mean ± SD of three experiments (*$P < 0.05$ versus value in Co, **$P < 0.01$ versus value in Co).

the axotomized facial motor nuclei of CS−/− mice (Fig. 6B). In contrast, intense immunoreactivity for CB was observed in the facial motoneurons but not in the perineuronal microglia of wild-type mice (Fig. 6C). Interestingly, the immunoreactivity for CB markedly increased in activated microglia abutting injured motoneurons in CS−/− mice (Fig. 6D). In contrast, immunoreactivity for CysC increased in activated microglia on the axotomized side of facial motor nuclei from both groups (Fig. 6E,F).

Decrease in Facial Motoneuron Survival following Axotomy in CS−/− Mice

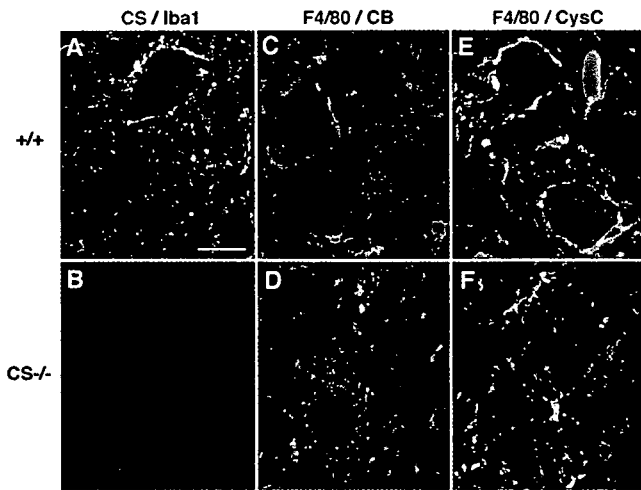Finally, we examined the effects of CS deficiency on axotomy-induced facial motoneuron death. On days

Fig. 6. Localization of CS, CB, and CysC in activated microglia that adhered to injured facial motoneurons 7 days after axotomy. A: Immunofluorescent CLSM image of CS (green). Scale bar = 25 μm. B: Immunofluorescent CLSM image of Iba1 (red). C: CLSM image of F4/80 (green). D: CLSM image of CB (red). Immunoreactivity to CB was observed in microglia abutting the facial motoneurons of CS−/− mice but not in the perineuronal microglia of wild-type mice. E: CLSM image of F4/80 (green). F: CLSM image of CysC (red). Immunoreactivity to CysC was observed in microglia of both groups.

Fig. 7. Decrease in facial motoneuron survival following axotomy in CS−/− mice. A: Immunofluorescent CLSM image of ChAT-positive facial motoneurons on control (Co) side of wild-type mice. Scale bar = 150 μm. B: Immunofluorescent CLSM image of ChAT-positive facial motoneurons on axotomized (Ax) side of wild-type mice. C: Immunofluorescent CLSM image of ChAT-positive facial motoneurons on Co side of CS−/− mice. D: Immunofluorescent CLSM image of ChAT-positive facial motoneurons on Ax side of CS−/− mice. E: Mean cell survival ratio of ChAT-positive facial motoneurons 4, 7, 30, and 50 days after axotomy in CS−/− and wild-type mice. Each column and bar represents the mean ± SD of four experiments (*significant difference between the 2 groups at $P <$ 0.05). Five serial sections (30 μm thick) stained with anti-ChAT antibody were prepared from each group. CLSM images of ChAT-positive facial motoneurons in each section were taken as a stack at 1-μm step size along the z direction with a 20X objective. The number of ChAT-immunoreactive cells in the facial motor nucleus of each section was determined, and the values of all the serial sections of an entire facial motor nucleus were summed.

4, 7, 30, and 50 after axotomy, we counted the ChAT-positive facial motoneurons on both the control and axotomized sides of the facial motor nuclei from the mice in both groups. As shown in Figure 7, the difference between the two groups was statistically significant ($P <$ 0.05) 30 and 50 days after axotomy. The mean percentage of ChAT-positive facial motoneurons that survived in wild-type mice 30 days after axotomy was 79.9% ± 2.3% (2,123 ± 65 cells on the control side, 1,697 ± 42 cells on the axotomized side), and the mean percentage that survived 50 days after axotomy was 69.7% ± 2.2% (2,204 ± 61 cells on the control side, 1,536 ± 44 cells on the axotomized side). The mean percentage of ChAT-positive facial motoneurons in CS−/− mice 30 days after axotomy was 60.7% ± 3.3% (1,917 ± 46 cells on the control side, 1,164 ± 39 cells on the axotomized side), and the mean percentage that survived 50 days after axotomy was 59.7% ± 2.6% (2,315 ± 43 cells on the control side, 1,382 ± 50 cells on the axotomized side).

DISCUSSION

Impairment of Migration and Transmigration of Activated Microglia and Monocytic Cells in CS−/− Mice

Following axotomy, microglia can become activated and therefore come into direct contact with injured motoneurons and begin to proliferate without turning into phagocytes (Ravich et al., 1999; Moran and Graeber, 2004). There is increasing evidence that the recruitment of monocytic cells through the cerebral vasculature and
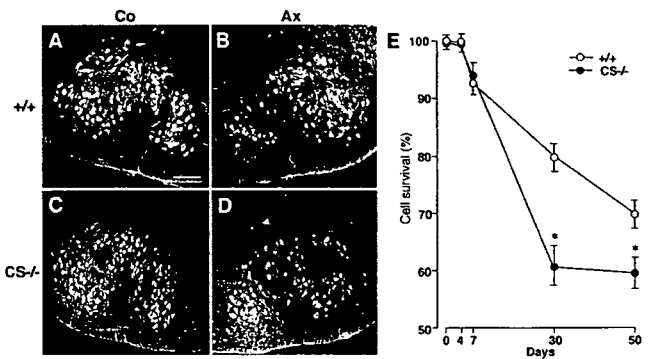
the leptomeninges also contributes to the increased number of microglia (Priller et al., 2001; Bechmann et al., 2005). In the present study, we found that cellular responses of microglia to facial nerve axotomy were markedly impaired in CS−/− mice. The mean number of activated microglia that accumulated on the axotomized side of facial motor nuclei of CS−/− mice was significantly smaller than that on the axotomized side of facial motor nuclei of wild-type mice. Furthermore, the activated microglia the accumulated on the axotomized side of facial motor nuclei of CS−/− mice exhibited some characteristics similar to those of phagocytic cells.

These observations show that the expression profiles of CB and CysC on the axotomized side of facial nuclei of CS−/− mice were quite different from those of wild-type mice. After axotomy, CB increased as the mature forms of activated microglia accumulated in the facial motor nuclei of CS−/− mice, but not in wild-type mice. CysC also significantly increased in activated microglia accumulated in the facial motor nuclei of both groups following axotomy. However, the expression of CysC on both sides of the facial motor nuclei of CS−/− mice was significantly smaller than that in wild-type mice. CB is known to increase in stimulated peripheral macrophages and phagocytic microglia in the CNS. More recently, CB has been demonstrated to be a major neurotoxic molecule released from activated microglia (Kingham and Pocock,